

EVALUATION OF MATERIALS IN ENTRY HEATING SIMULATION

By William A. Brooks, Jr.

NASA Langley Research Center  
Langley Station, Hampton, Va.

Presented at Conference on the Role of Simulation  
in Space Technology

FACILITY FORM 606	<b>N 65 16154</b> (ACCESSION NUMBER)	_____	(THRU)
	<u>54</u> (PAGES)	_____	1 (CODE)
	<u>TMX-54976</u> (NASA CR OR TMX OR AD NUMBER)	_____	<u>33</u> (CATEGORY)

Blacksburg, Virginia  
August 17-21, 1964

GPO PRICE \$ \_\_\_\_\_

OTS PRICE(S) \$ \_\_\_\_\_

Hard copy (HC) 3.00

Microfiche (MF) .50

# EVALUATION OF MATERIALS IN ENTRY HEATING SIMULATION

By William A. Brooks, Jr.  
NASA Langley Research Center

## INTRODUCTION

The basic objective in designing thermal protection systems is the provision of sufficient material to protect the vehicle structure and cargo from the severe heating encountered during entry into a planetary atmosphere. Conservative designs that may compromise the mission objective should be avoided. Ideally just enough material to ensure successful entry should be provided. The degree of success that is achieved by adhering to this philosophy is entirely dependent upon our knowledge of the entry environment and the manner in which the various materials respond to the environment.

The importance of avoiding excessive heat shield weight can be underscored by reference to figure 1 (ref. 1). Of course, the basic problem of reentry is the dissipation of a vehicle's energy in a controlled and acceptable fashion. This figure was prepared to qualitatively demonstrate the influence of thermal protection weight upon the useful payload capability.

The ordinate is energy in Btu/lb and the abscissa is velocity, covering the range of concern for manned vehicles and planetary probes. The solid line is the kinetic energy per pound of vehicle which must be dissipated at each velocity. Fortunately, most of the energy is absorbed by the atmosphere which envelops the entering vehicle. At most, only a few percent of the kinetic energy is transferred to the vehicle in the form of heat. The lower cross-hatched band represents the total heat load per pound of vehicle. The lower edge of the band corresponds to less than 1 percent and is typical of the heat load for a ballistic reentry. The upper edge is about 3 percent of the kinetic energy which is typical for lifting entry vehicles. At the higher velocities, radiative heat transfer from the hot gas cap becomes significant and increases with velocity, resulting in large increases in heat load. The cross-hatched horizontal band represents the energy absorbing capability of thermal protection materials and ranges from 2,000 to 20,000 Btu/lb.

Now if the vehicle heat load is equal to the heat shield energy absorbing capability, that is, the two bands coincide, then the vehicle must be constructed entirely of thermal protection material in order to survive the heating. Therefore, the difference between the two bands indicates the amount of vehicle weight which can be devoted to functions other than thermal protection. As velocity increases, the useful payload capability becomes smaller, and the matter of excessive heat shield weight becomes more critical.

## REQUIREMENTS FOR DUPLICATING THE ENTRY ENVIRONMENT

If it were possible to duplicate the reentry environment in ground facilities, the manner in which thermal protection materials respond could be more precisely determined and better heat shield designs would result. However this is not generally the case and usually one must resort to a partial simulation.

Figure 2 shows the flight regions of immediate concern in an altitude-velocity plane (ref. 2). Regions are shown for Apollo, ICBM's, Mercury, and Dynasoar. A slight broadening of the Dynasoar band will result in a region which is typical of hypersonic gliders. Future planetary exploration vehicles will result in a region whose lower bound may be as much as 50,000 feet below the Apollo region near escape velocity, extending off-scale to the right.

Figures 3, 4, and 5 show some of the wind-tunnel characteristics that would be required to produce exact flow duplication (ref. 2). First consider the chamber pressure required (fig. 3). Pressure curves have been superposed on the flight regions shown in figure 2. The technology of building pressure vessels of the size required by a wind tunnel and pumps probably provides a pressure limitation somewhere between  $10^4$  and  $10^5$  psi. In any event, the limitation is remotely removed from the point of maximum heating for Apollo which is about 32,000 fps.

Figure 4 shows the mass flow rate that would be required per square foot of test section. It can be seen that the required flow rate is not a strong function of entry velocity but is influenced by the simulated altitude. The small and moderate flow rate curves pass through the Apollo region. However, a very substantial flow rate is required for the ICBM region.

Figure 5 shows the heat energy required per square foot of test section to provide a duplication of enthalpy. It is to be noted that this is the energy in the air and that the energy supply must be 2 to 3 times as great because of the losses incurred during transfer to the air. At the higher altitudes where small and moderate mass flow rates are adequate, the energy requirement can be met without difficulty. However at the lower altitudes which require large mass flow rates, the power requirement is prohibitive.

At the NASA Langley Research Center with the existing power distribution system, it is possible to draw a maximum of 100 megawatts. Assuming about 50 percent efficiency, a device with 1 square foot of test section could be powered at an energy level that would approximately coincide with the lower bound of the Apollo region.

Exact duplication of the stagnation flow condition is out of the question, mainly because of the pressure requirements.

## FACILITIES FOR SIMULATING CONVECTIVE HEATING

The type of facility most commonly used to evaluate thermal protection materials is that which utilizes an electric arc for adding energy to the gas stream. Figure 6 shows the capabilities of arc facilities presently being used. In this figure, the limitations of present facilities have been plotted in terms of arc chamber pressure and enthalpy, the two most important parameters in an arc-heated wind tunnel (ref. 3).

One of the principal factors that limits the capabilities of present facilities is the energy losses which result from thermal radiation from hot, high-pressure gases to the walls of the arc chamber. This problem area has not yet been well researched. Perhaps a more fundamental difficulty is the inability to sustain an arc in a moving gas stream at high pressures.

Another problem area results from the cooling requirements for the nozzles. The dashed line is an estimate of a practical limitation and approximately corresponds to nozzle heating of 10,000 Btu/ft<sup>2</sup>-sec.

The stringent requirements of exact duplication of high-velocity entry is indicated for the altitude range of 100,000 to 300,000 feet and quite obviously will not be achieved with present techniques. If one is willing to relax the Mach number requirement and settle for a partial simulation, the indicated shaded area results. Even this partial simulation of a low-altitude flight cannot presently be achieved for high-entry-velocity situations.

This point can be made more directly by superposing the exact and partial simulation capabilities of present facilities on the flight regions as shown by figure 7. Our attempts to simulate all the quantities of interest cover only a small portion of the flight regions.

As yet no mention has been made of size and it is pertinent to point out that certain of the entry effects such as heating rate, aerodynamic shear, etc., are dependent on the size and geometry of the specimen. Further complications result because the mass flow characteristic of presently available facilities greatly limits the size of the specimens.

So one is confronted with partial simulation of a few of the entry heating parameters in a given test, a scaled-down specimen, but generally with full-scale heat shield materials. It is not possible to model with a different material because of the dissimilarity of material response in a given environment. The heat shield material thickness is generally not scaled because a given heating environment requires a given thickness regardless of the specimen size.

The usual technique is to conduct a series of tests in each of which a few parameters are simulated. Then analysis or other test results are employed to indicate the degree that the interaction between the parameters influences material response.

Figure 8 shows the test stream configurations commonly employed for materials testing with arc air heaters (ref. 4). Free jets, which exit to the atmosphere, are used in both subsonic and supersonic arrangements. The pressure at the model is atmospheric pressure or greater. The splash technique is the simplest and one of the more commonly used techniques. The heated stream and the specimen are sized so that the stream impinges on the specimen rather than enveloping it. This condition affords a simulation of stagnation-point heating conditions. Some attention must be devoted to preventing heat flow into the sides of the specimen if stagnation-point heating is to be realistically simulated. The splash technique is utilized in material screening and evaluation programs and in instrumentation studies.

The arc tunnel arrangement is utilized for the consideration of locations other than the stagnation point. The stream is expanded and discharged into an evacuated plenum chamber. Expansion of the stream results in the capability of enveloping rather large specimens with a hot gas stream. The pressure at the specimen can be less than atmospheric, thus simulating high altitudes.

The technique of shrouding the test model is utilized to produce subsonic flow ahead of the model. With a given mass flow, more of the hot gases can be brought into contact with the specimen. The result is that for a given flow situation larger specimens can be tested. This technique is employed to study the effects of pressure gradients and other phenomena associated with two- and three-dimensional stagnation areas.

The pipe flow technique consists of utilizing the test specimen in the form of a simple or internally contoured pipe through which the gas stream flows. This method of testing materials has been used to determine the effects of flow on the test material. The shape of the pipe and the flow parameters can be selected so that turbulent flow results. Thus the interaction between an ablation material and turbulent flow can be investigated.

#### FACILITIES FOR SIMULATING COMBINED RADIATIVE AND CONVECTIVE HEATING

Up until the present time, entry velocities have generally been sufficiently low that entry heating has been essentially a convection process. For entry near earth satellite speed, the radiative component is negligible - except for the ICBM's which plunge deep into the atmosphere. As the entry velocities become greater, the air in the bow shock layer becomes excited to the point where it becomes a powerful source of radiative heating. At escape velocity, radiative heat transfer is a significant part of the heating. For planetary exploration vehicles that reenter the earth's atmosphere at very high speeds - well above escape velocity - radiative heating can become the dominant mode.

At present, most of the experimental research on thermal protection materials is carried out in facilities that provide only convective heating. Arc image furnaces are used to provide radiative heating only. It is a generally accepted view that even in those cases where radiative heating is the dominant mode some convection at the heated surface is required for proper simulation.

Only in a few instances have there been attempts to provide combined convective and radiative heating.

The next few figures show known existing devices for providing combined heat. Figure 11 shows a device used at Langley (ref. 5). A resistance heated graphite sleeve was placed in tandem with the output from an arc jet, providing radiative inputs to the specimen up to 200 Btu/ft<sup>2</sup>-sec. This device is unsatisfactory because the jet stream consumes the graphite heater resulting in frequent replacement. In addition, because of the presence of large amounts of carbon in the stream, the chemistry at the surface of the ablating specimen is not correct. Lastly, the radiative rates available are not high enough.

The Ames Research Center is using a device (ref. 6) which couples an arc image furnace to a small arc jet, producing the radiative rate shown in figure 12. The output from the carbon arc is refocused on the specimen by means of mirrors with the output being controlled by a shutter, screen, and filter arrangement. An advantage of this type of arrangement is that the radiative and convective heating are independently controlled. However, the radiative rate shown represents about the maximum that can be achieved with arc image furnaces.

Another device is shown in figure 13. This device is employed by the General Electric Company and is essentially a long constricted arc (ref. 7). The test gas is heated by the arc and expelled into the plenum chamber and through the nozzle. The model is positioned so that it receives radiative heating from the arc and the plenum chamber gases. The maximum radiative rate is obtained when the specimen completely blocks the flow and the bypass port is used to discharge the heated air. By selective positioning of the specimen and adjustment of the bypass port, various combinations of convective and radiative heating are obtained. The technique involves the use of the same arc to provide both radiative and convective heating. The disadvantages are the relatively low radiative rate and the coupled control of convective and radiative heating.

Figure 14 shows a device which reportedly affords a very high radiative heating rate. In this device the material specimen serves as the chamber that confines the arc which radiates directly to the test material. The radiative rates are calculated to be as shown. However, the only gases involved are those generated when the test material decomposes. These gases exit around the electrodes as shown and reportedly produce a stagnation area type of flow at the center of the specimen. It is evident that the convective heating and the surface chemistry are not correct.

In another version of the technique of using the test material to confine the arc, the arc and test gases are passed through a cylinder of test material which confines the arc and the gas flow. The test material thus constitutes a portion of the constrictor.

There are shock tunnels both existing and proposed, modified in various ways, that produce good simulation of the high-speed thermal environment. However, testing is restricted to very small models and to test times measured in

microseconds. Thus, although the shock tube facilities are extremely valuable in research on the physics and chemistry of air, they are of little value for testing materials. The one known exception is the Cornell Aeronautical Laboratory's Wave Superheater. The superheater which utilizes a sequential firing of many shock tubes provides good simulation up to about  $M = 14$  with test times as great as 15 seconds.

## RESPONSE OF ABLATIVE MATERIALS TO SIMULATED ENTRY ENVIRONMENTS

Research has shown that two of the important characteristics of a good heat shield material are the ability to sustain high surface temperatures so as to reject heat by reradiation and good insulative properties so as to delay heat penetration to the interior of the vehicle.

### Charring Ablators

A class of materials which has been shown to have these characteristics are the so-called charring ablators. Charring ablators function in a very complex manner. In addition to being related to each other, the basic processes and mechanisms which are brought into play are intimately related to the aero-thermal environment. Therefore the type of test simulation influences the material response.

Some of the details of a charring ablator are shown in figure 15 (from ref. 8). The charring composites, in general, consist of plastic resins - such as phenolic, epoxy, and silicone - filled with organic or inorganic materials in the form of powder, fibers, or cloth. On the left are typical layers which result during ablation. At the bottom is the structural substrate to which the virgin composite is bonded. Above the virgin material is the pyrolysis zone at which, due to the influence of heat, the virgin material decomposes into gases and a carbonaceous residue. As the decomposition proceeds, the carbonaceous layer, or char, reinforced by the filler materials builds up to an appreciable thickness. Finally, if glassy filler materials are used, a melt layer may exist.

On the right are some of the processes which take place during ablator. Pyrolysis takes place at the relatively low temperature. Thus the potential for heat conduction is not very large and if the diffusivity of the virgin material is sufficiently low the temperature response of the structure is slow. When pyrolysis takes place the degradation process serves as a heat sink. However the heat of degradation is generally small compared to the amount of heat that must be accommodated overall by the ablator. The pyrolysis gases percolate, or transpire, through the char picking up heat in the process. There is also a possibility that reactions may take place between the gases and the chars or between the various gaseous species. Within the char, conduction of heat toward the pyrolysis zone is partly canceled by action of the transpiring gases. The gases are then injected into the boundary layer, thereby blocking convective heat transfer to the surface. As the char layer

becomes thicker the surface temperature rises and a large amount of heat is rejected by reradiation to space. The char is then eroded by thermal, chemical, or mechanical means such as sublimation, oxidation, or removal by aerodynamic shear.

Basic equations governing the response of charring ablators are shown in figure 16. At the top, the surface energy balance, or boundary condition, is given. The convective heating is reduced by the hot wall correction and the blocking effect of the transpiring gases. Next is that portion of the radiative heating which is absorbed. For present materials, this is usually most of the radiative heating because the reflectivity of the charred surfaces is low. The next term is the heat input which results from the oxidation of the char. There might also be another term here which results when the pyrolysis gases undergo a homogeneous combustion reaction in the boundary layer. On the right side is the reradiative term which is very important for charring ablators, conduction into the interior of the heat shield, and a term to allow for the sublimation of the char which may take place if the temperature is sufficiently low. The effects of pressure and aerodynamic shear are not shown here - mainly because there is very little experimental evidence to indicate how these mechanisms must be treated. At present, they are usually treated with auxiliary equations which specify a maximum char thickness.

An energy balance on the degrading material produces the very general equation shown here. Except for the term which accounts for heat disposed of by convective transport, the equation is similar to the diffusion equation. This equation probably overly simplifies the mathematical formulation of the problem as many auxiliary equations are required to account for all of the mechanisms.

### Instrumentation of Ablators

One of the primary difficulties that is experienced with the experimental evaluation of charring ablators is that several effects take place simultaneously and what one sees when the test is completed is the combined, or overall, effect. During the course of the test, the receding char surface is usually obscured by the pyrolysis gases or the air stream and therefore motion pictures do not yield much quantitative information.

In the past, the principal type of instrumentation utilized in ablation tests has been thermocouples. However, even when thermocouples are used the utility of the data is limited and, in fact, sometimes erroneous. Figure 17 has been prepared to illustrate the latter point. There is shown a sectioned test specimen which was instrumented with complete disregard for the basic rules of thermometry. The thermocouples were positioned with the axes of the wire in the direction of the flow of heat. The thermocouples are much better conductors than the virgin plastic as is evidenced by the degradation of material along the wire. There can be no doubt that erroneous temperature readings were obtained in this test.

Figure 18 shows quantitatively the effect of thermocouple configuration. Configuration (1) consists of a grooved plug with a wire running down each

side. The wire insulation is removed and replaced with ceramic tubing. At the end of the plug, the bare wires are joined at the center. Several diameters of the wires are perpendicular to the heat flow direction to minimize the conduct effects. Configuration (2) consists of a thermocouple potted in a hole whose axis is parallel to the heat flow. In this case, the wire insulation is replaced with two-tube ceramic tubing. Configuration (3) is similar to configuration (2) with the exception that the resin-glass insulation is left on the thermocouple wire. The difference between the response of sensors (1) and (2) shows the effect of thermocouple configuration with the temperature difference being as much as  $1500^{\circ}$  F. The difference between the responses of sensors (2) and (3) results from the difference between the conductivities of the wire insulation and the ceramic tubing.

Even the use of correct thermocouple technique does not yield as much information on the performance of charring ablators as is desired. Among the items one would like to see recorded during a test are the surface recession and the char thickness. The Instrument Research Division at Langley has been studying instrumentation for ablators and has devised some rather promising sensors using simple techniques.

Figure 19 shows a make-wire gage. Make-wire gage techniques have been utilized before but with rather limited success. This version, which is intended to sense the interface between the virgin material and the char, shows considerable promise. Ten-mil platinum wires are positioned as shown in a split plug of the plastic material. Noble metal is used to prevent the formation of conductive oxides. It has been found essential topeen the ends of the wires to make good contact with the char. As the front of material degradation passes the ends of the wire the electrical conductivity of the material in contact with the ends increases and the circuit is completed through the char. Conditioning circuitry is used to provide a constant voltage step indicating the event.

A gage for sensing the surface recession is shown in figure 20. A tungsten wire is attached to one leaf of a spring-loaded microswitch. The wire is threaded through a molybdenum tube and knotted in such a fashion that the switch is open. As the surface recedes toward the end of the sensor the temperature increases to the point where the tungsten melts and the switch is closed by the spring, giving a voltage indication of the event. Tungsten melts at about  $4700^{\circ}$  F so this is actually a temperature indicator. However, the temperature gradients are very steep near the surface and therefore the  $4700^{\circ}$  F isotherm corresponds very closely to the surface location. In principle, one would make the wire refractory enough to ensure the surface being reached but of small enough mass so that it would melt immediately upon exposure at the surface.

Another type of surface sensor is shown by figure 21. This is a light pipe sensor which consists of a sapphire light pipe, an infrared filter, and a photo-resistive diode. The diode decreases in resistance with increasing light. The infrared filter is used to make the gage less sensitive and more capable of a sharp output. At  $1000^{\circ}$  F there is essentially no output from

this gage. As the end of the light pipe approaches the surface due to the rapidly increasing temperature an output results.

Figure 22 shows the determination of char thickness with these gages. Recession of the char interface was sensed by the make-wire gage and recession of the surface by the light pipe sensor. The difference between the two readings gives the char thickness as a function of time. The magnitude and steady-state char thickness were verified by measurements of char thickness on sectioned specimens tested for 10, 20, and 30 seconds.

In addition to sensors such as these, research is being performed by several organizations on sensors which utilize radioactive elements. The change in measured radioactivity is used as a means of locating the surface and the char interface.

The most careful simulation of entry heating on a charring ablator will not yield the detailed information regarding the ablation processes unless suitable ablation sensors are developed.

#### Effect of Radiative Heating

Unfortunately there is a dearth of useful experimental data from combined convective and radiative tests - principally because of the lack of adequate facilities. Figure 23 shows some results obtained by Langley using the resistance-heated graphite radiator previously described (ref. 5). The efficiencies of three materials - Teflon, Fluorogreen, and phenolic-nylon - are given as a function of the total cold-wall heating rate. Efficiency or effectiveness will be used in succeeding figures and is defined as the total cold-wall heat input which can be accommodated by a pound of material before reaching a specified back-surface temperature - which was 300° F in this case. Data are shown for radiative heating alone, convective heating alone, and combined convective and radiative heating. Briefly, when teflon experiences radiative heating alone or combined radiative and convective heating its efficiency drops considerably from the level that would have been obtained with convective heating only. This is attributed to the thermal transparency of teflon. Fluorogreen is essentially Teflon with additives that increase the opaqueness to thermal radiation. Although the result with convective heating alone is the same as for Teflon, radiative heating produces much less decrease in efficiency.

Finally, for the phenolic-nylon material, it is seen that over the test range of heating rates about the same efficiency is obtained regardless of the type of heating. However these results are not believed to be indicative of what would happen in a flight situation. In these tests the enthalpy was quite low and therefore the ablation blocking mechanism was not very significant. Inasmuch as it is this blocking mechanism that is most affected by radiative heating, the simulation was not adequate.

Figure 24 shows some calculated results (ref. 11) which probably provide a clearer picture of the effect of radiative heating. The ordinate is dimensionless heat of ablation, which is a gage of material performance, and is

defined by the equation where  $q_0$  is hot-wall convective heating rate to a nonablating body and  $q_r$  is the net radiative heating. The abscissa is the dimensionless enthalpy difference. The quantity  $q_r/q_0$  is the ratio of the net radiative heating - that is, the radiative input minus reradiation - to the hot wall convective rate. The curve marked for the zero value of the ratio is for convective heating only. As the ratio increases, the heat of ablation decreases by a substantial amount. This results because the gases that the ablating surface injects into the boundary layer generally do not block radiative heating. More mass is injected into the boundary layer than would be the case if all the heating were convective. Negative values of the ratio result when the reradiative rates are higher than the radiative input. In this instance, there is an increase in heat of ablation. Thus it can be seen that the effect of radiative heating depends critically upon the relative magnitudes of the radiative and convective heating and the enthalpy difference.

Another aspect of this problem is the effect of radiative heating in a situation where char oxidation is significant as it may be for charring ablator. At the higher temperatures, oxidation is a function of the rate of diffusion of oxygen to the surface. In turn, the diffusion of oxygen is related to convective heating. Just as mass injection blocks convective heating, it also interferes with the diffusion of oxygen to the ablator surface. Therefore, the mass injection which results from the radiative component of heating will lessen the char oxidation. Combined radiative and convective heating should result in less severe oxidation than an equal amount of convective heating only.

#### Effect of Convective Heating

Heat shield efficiency changes greatly with variation of the entry environment and the various materials respond differently to these variations as shown by figure 25. In each of the four graphs, the change in thermal efficiency of two good heat shield materials is plotted as a function of changes in an important environmental; for example, an increase in velocity, or enthalpy, from orbital to escape speed, such as going from the Mercury to the Apollo mission. Also considered are changes in the heating rate, surface oxidation, and shear.

Figure 26 shows qualitatively the effect of oxidation on char erosion. The sectioned specimens shown here were tested in an arc jet condition that was not energetic enough to remove char by means of pressure or shear forces. In addition, the surface temperatures experienced by these specimens were not high enough to result in the sublimation of char. The principal means of char erosion was oxidation.

The specimens were made of the same material and were of the same shape and size. They were subjected to the same heating conditions for the same period of time. The only differences in the tests were the oxygen percentages of the stream. The original specimen outlines are shown for reference purposes.

The specimen on the left was tested in a 100-percent nitrogen stream. This specimen, which shows a small change in size and practically no change in shape, lost about 47 percent of the original mass. The small change in size is believed to have resulted from shrinkage which occurs when this material pyrolyzes. The specimen in the middle was tested in a stream whose content by weight was 90-percent nitrogen and 10-percent oxygen. The change in size is more substantial and there is a significant change in shape. The total mass loss in this test was about 56 percent. Finally, the specimen on the right was tested in air. Here there is a drastic change in size and shape. The mass loss for this case was 68 percent. A closer examination also reveals that the char thickness is inversely related to the oxygen content with the thickest char being developed in the nitrogen stream.

Effects such as these have a marked influence on the efficiency of a material as can be seen in figure 27. Thermal effectiveness of a phenolic-nylon material is plotted as a function of cold-wall heating rate for tests in streams of four different compositions. For tests in air, the effectiveness is about 6000 Btu/lb and is a very weak function of heating rate. For tests in nitrogen, the effectiveness is from 2 to 3 times as great as obtained in the tests in air for the range of heating rates shown and is strongly influenced by heating rate.

Figure 28 shows a comparison of calculated and experimental oxidation effects. In this case, the material effectiveness is plotted as a function of stream oxygen content for a single heating rate. Calculated data are shown for enthalpies ranging from 3,000 to 25,000 Btu/lb - corresponding to a low enthalpy test condition and the enthalpy associated with entry at escape velocity. Experimental data taken at 3,000 Btu/lb indicated fair agreement between experiment and theory. More important, however, is the conclusion that the major oxidation effects occur at the lower enthalpies.

If high enthalpy char oxidation is to be simulated in a low enthalpy facility, the stream oxygen content must be reduced. Tests in air would indicate a more deleterious effect than would be obtained in flight. This also emphasizes the attention which must be given to producing the proper surface chemistry when simulating heating.

The oxidation effect just shown for phenolic nylon might not appear when dealing with another material. Figure 30 shows the results of a similar series of tests on a silicone resin with glass fillers. Again effectiveness is plotted as a function of heating rate. The first thing to note here is that the stream composition generally speaking has a rather negligible effect on the performance of the material. However this material does show a heating rate effect. When this material ablates, a glassy layer is formed at the surface. As the heating rate, and in turn the surface temperature, increases, the glassy layer becomes less viscous and is rapidly removed by aerodynamic forces. The maximum efficiency is produced at about 150 Btu/ft<sup>2</sup>-sec.

If one were considering this material and the previously discussed phenolic-nylon material for a flight application and made screening tests in air to determine which material was best, he might erroneously conclude that the silicone material was much better than the phenolic-nylon material.

Actually, if proper consideration is given to the fact that the test of phenolic nylon in air is more severe than would be experienced in flight, one concludes that up to a heating rate of  $150 \text{ Btu/ft}^2\text{-sec}$  the efficiencies would be about the same.

Figure 30 shows a comparison of calculated and experimental heating rate effects for the silicone material. The experimental data curve is the average of data taken at  $3,000 \text{ Btu/lb}$ . Calculations are shown for two enthalpies,  $3,000$  and  $25,000 \text{ Btu/lb}$ . The test specimens on which the experimental data were taken had calorimeters on the back surfaces. The calculations shown here do not include the effect of the calorimeter. However since this figure was made, the effect of the calorimeter has been included and the calculated curve for  $3,000 \text{ Btu/lb}$  shifted slightly to the right and slightly above the data curve shown here. The significant feature of this figure is the indication that it is possible to analytically predict the heating rate effect. If one can predict test results, one can extrapolate to conditions more severe than the test environment with much greater confidence.

#### Mechanical Erosion of Char

The next item to be discussed is the erosion of char by aerodynamic shear. This is a phenomenon that is not presently well understood but which can be demonstrated to be very significant. Manned vehicles experience long heating periods and in order to improve ablation material insulative qualities so as to provide protection for long heating times, there has been a trend toward decreasing material density. This has been shown to increase the effectiveness of the materials. However the chars which are produced by the low-density materials may be quite fragile. Even the low to moderate shear forces experienced in a manned entry may result in substantial erosion of the char and a drastic decrease in the material efficiency.

Figure 31 shows sectioned test specimens subjected to different shear levels. Two materials were tested, a molded phenolic-nylon and a glass reinforced epoxy resin. The phenolic material was  $36 \text{ lb/ft}^3$  and the epoxy material was about  $32 \text{ lb/ft}^3$ . However there was a vast difference in char strength as is indicated here. The original specimen profiles are shown for reference purposes. At the low shear level, the phenolic material experienced no difficulty, whereas the epoxy material experienced significant erosion. At the high shear level, the difference in performance is greatly magnified - particularly when one notes that the phenolic material was exposed about four times as long.

The reason for pointing out these shear tests is that, in the past, experimenters have been obsessed with producing high enthalpy test devices. In many instances, the high enthalpy devices utilize very low mass flows and produce negligible shear on specimens. Phenomena such as shown here can be completely overlooked in such cases.

As a matter of fact, some thought is now being devoted to the consideration of duplication in terms of what the ablating surface feels rather than devoting so much attention to the simulation of free-stream parameters. Figure 32 shows some of the inputs to the surface of the material. The inputs are thermal, chemical, and mechanical. The thermal inputs shown here are the absorbed radiative heating and the net convective heating. The chemical input is the rate of diffusion of oxygen. The mechanical inputs are the pressure and the shear.

First-order approximations show that the inputs are related as shown. The denominators are the enthalpy, concentration, and velocity differences across the boundary layer.

Some preliminary testing has been done utilizing this approach. The results are shown in figure 33. A test was made in a high enthalpy facility which produced the test conditions shown here. Because the facility is newly installed and control equipment is presently lacking, the oxygen concentration was high. The test results obtained on a phenolic-nylon specimen were as shown. Calculations were made to determine what the test conditions, other than enthalpy, should be in order to produce similar results. A specimen tested under the calculated conditions in the low enthalpy facility produced the listed results which are quite similar to the high enthalpy results.

Figure 34 shows the sectioned test specimens to further demonstrate the similarity. Admittedly these are preliminary data, but it is believed that more attention should be devoted to this approach to simulation. It is quite possible that present facilities, limited as they are, can produce more meaningful test data.

#### FLIGHT TESTS OF ABLATIVE MATERIALS

Up to now, ground tests have been discussed exclusively. In spite of the vast number of ground tests, they are, at best, partial simulations of many effects. The final verification of a heat shield design, or of an analytical prediction, or a simulation technique, must be accomplished by flight tests. Flight tests provide the necessary confidence factor for the utilization of ground test results.

An example of the type of test of interest is the pending test of charring ablator in a high enthalpy reentry environment which cannot presently be simulated on the ground. The booster that is to be utilized in this test is the four-stage Scout booster. A fifth stage, in the form of a spherical rocket, is added to the payload. Two rockets are fired to propel the payload upward to the desired position and the remaining three rockets drive the payload into the earth's atmosphere at a velocity of about 28,000 fps. ( $\gamma \approx -7.5^\circ$ ,

$$\frac{W}{C_D A} \approx 165 \text{ psf.})$$

Figure 35 is a picture of the payload with the components separated. The 18-inch-diameter aft end of the payload is at the left of the photograph where interstage structure can be seen attached to the spherical motor. These components are separated before reentry. The instrumentation deck is to the right of the spherical motor. Next is the instrumentation deck housing. The white truncated cone is the payload afterbody which is constructed of magnesium covered with Teflon for thermal protection. The next component is the payload battery pack. The 11-inch-diameter payload nose cap at the extreme right is the primary experiment. A low-density charring ablator is bonded to a steel shell. The ablator is well instrumented with thermocouples and the previously described ablation sensors.

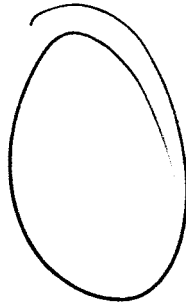
Considerable ground test data for the material were generated. In some of the tests, excessive char erosion was apparent. However, the actual failure mechanism could not be determined. Using available data, several organizations made predictions of how the material would perform in the flight test. The results were as shown in figure 36. The amount of heat shield material remaining is plotted against time, measured from the beginning of heating. The heating pulse is shown for reference purposes. The shaded band shows the range of predictions. At the top edge of the band where success is predicted, the prediction procedure was almost entirely empirical to the extent of employing an unrealistic ablation model with empirically determined characteristics. At the bottom edge of the band, the heat shield is predicted to fail before peak heating. In this case, a more reasonable ablation model was utilized with correlated test data to prescribe char removal. The data however were taken at conditions somewhat different from the entry environment. Several other predictions fell between these two extremes but most of them predicted failure near the end of heating.

This is a very graphic example of the wide variation in results that are obtained when test data are extrapolated considerably beyond the range of parameters of the tests in which the data are taken. However, it should be pointed out that the performance of this material could not be characterized to the desired extent before the predictions were made.

#### CONCLUDING REMARKS

The effects of several environmental parameters on the behavior of ablation materials have been examined. Practically all the entry heating parameters such as enthalpy, pressure, heating rate, aerodynamic shear, and so forth, affect material performance. However, the significance of the effects depends to a large extent upon the type of material. Inasmuch as it is rarely possible to simulate several environment effects simultaneously, the primary inputs must be determined and the test simulation must account for the effects of these inputs. The particular materials of concern must be characterized by test and analysis to determine which of the many environmental inputs are the most significant.

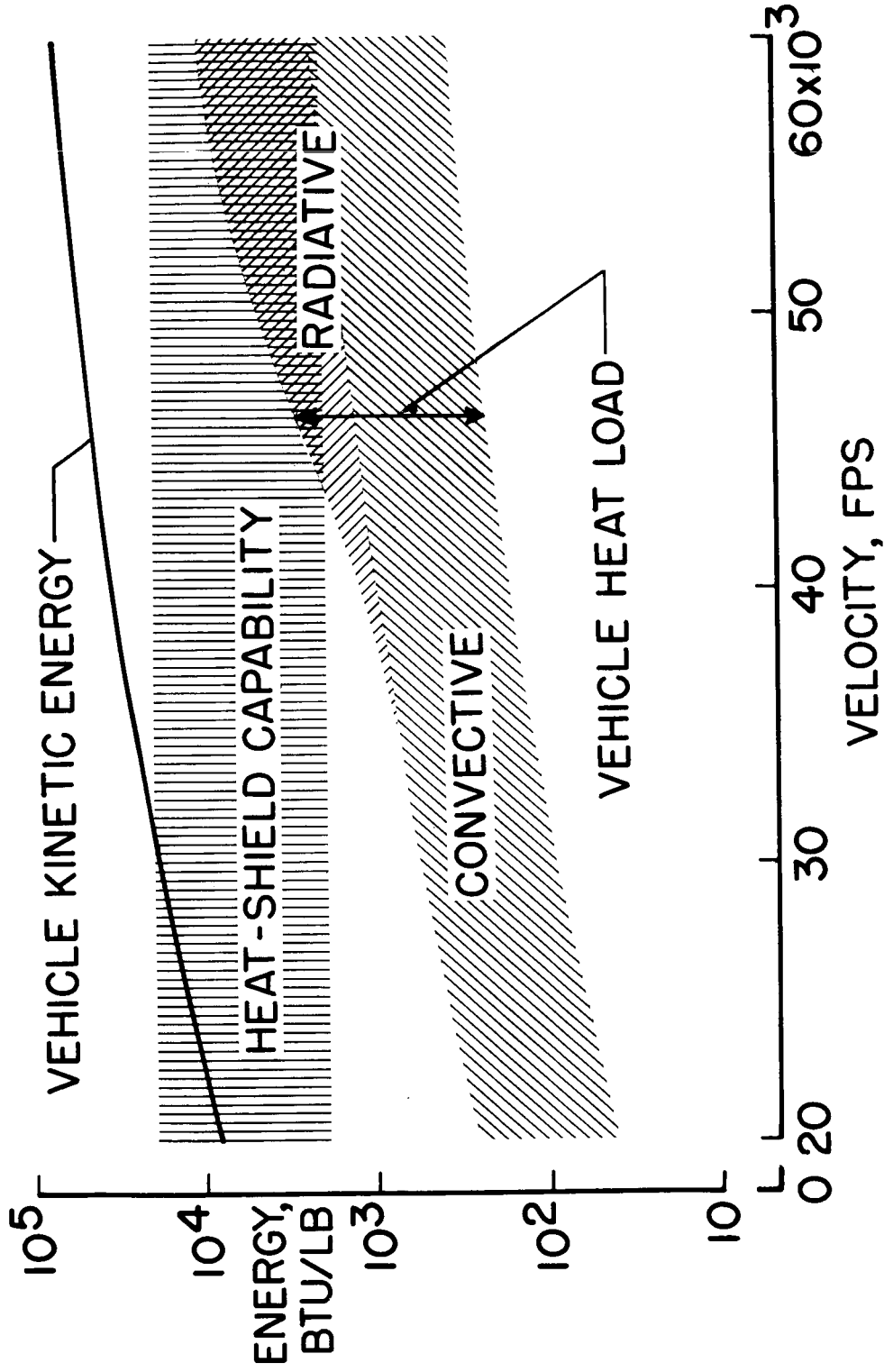
It must also be evident that extrapolation of experimental data to an environment considerably more severe than the test environment can lead to erroneous conclusions. Admittedly at the present time, extrapolation must generally be resorted to for the most advanced entry missions. However, by combining careful characterization of materials in less severe environments with analytical predictions of behavior in the flight environment, one may develop procedures that can result in adequate heat shield designs.



## REFERENCES

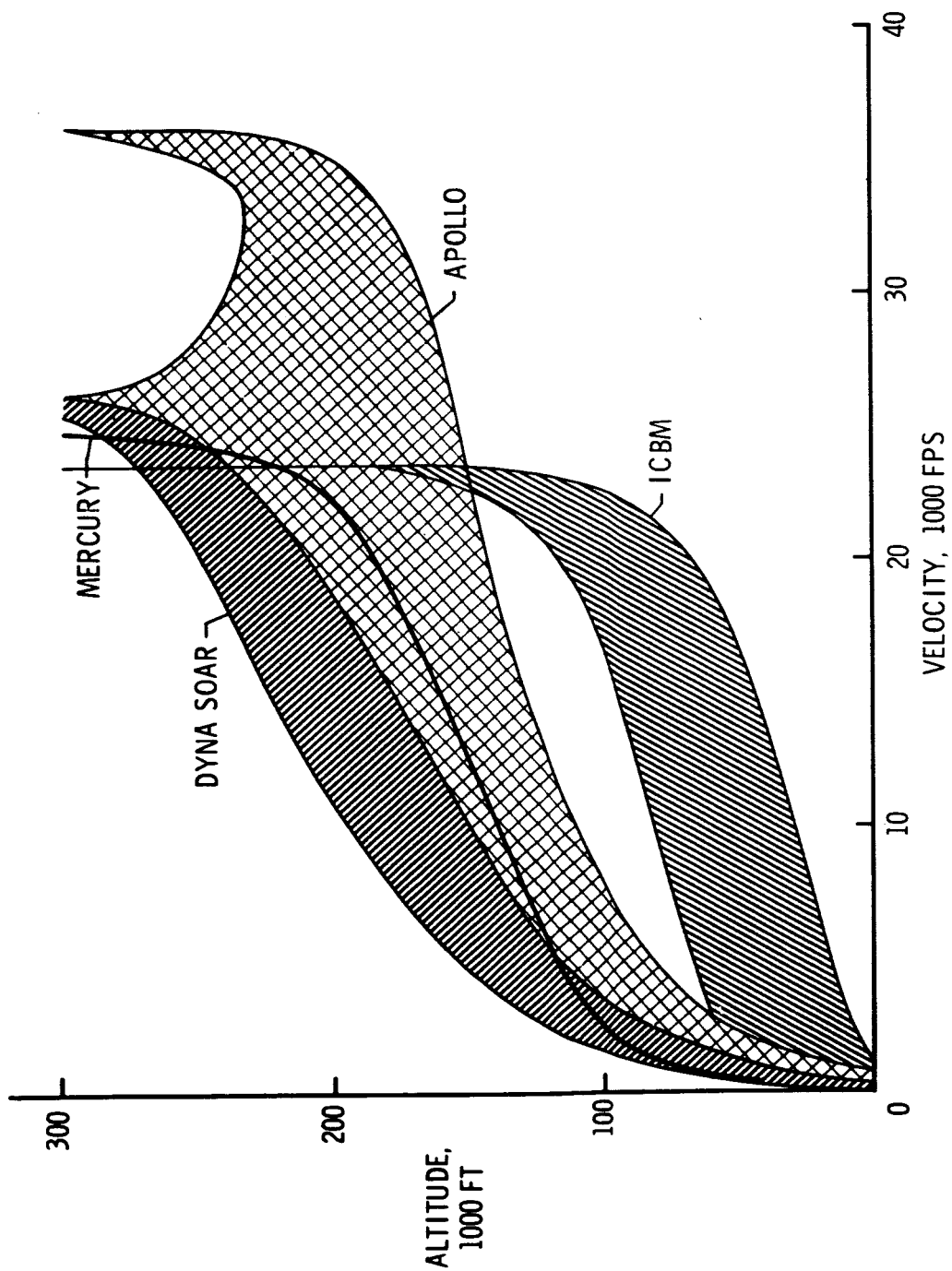
1. Anderson, R. A.: Research, Design Considerations, and Technological Problems of Structures for Planetary Entry Vehicles. Proceedings of the NASA-University Conference on the Science and Technology of Space Exploration, Chicago, Illinois, Nov. 1-3, 1962, vol. 2, NASA SP-11, pp. 511-519.
2. Heldenfels, R. R.: Ground Facilities for Testing Reentry Structures and Materials. Proceedings of the Conference on Physics of the Solar System and Reentry Dynamics, Virginia Polytechnic Institute Engineering Bulletin No. 150, Aug. 1962, pp. 315-338.
3. Cann, G. L.; Teem, J. M.; Buhler, R. D.; and Branson, L. K.: Magnetogas-dynamics Accelerator Techniques. Arnold Engineering Development Center, AEDC TR 62-145, July 1962.
4. Warren, W. R.: Laboratory Experimental Studies in Reentry Aerothermodynamics. General Electric Company, Missile and Space Vehicle Dept., Rept. TIS R59 SD 362, 1959.
5. Brooks, W. A.; Swann, R. T.; and Wadlin, K. L.: Thermal Protection for Spacecraft Entering at Escape Velocity. Society of Automotive Engineers Preprint 513 F, Apr. 1962.
6. Lundell, J. H.; Winovich, W.; and Wakefield, R.: Simulation of Convective and Radiative Entry Heating. Symposium on Hypervelocity Techniques, Denver, Colorado, Mar. 20-21, 1962.
7. Diaconis, N. S.; Weber, H. E.; and Warren, W. R.: Technique for Severe Radiative and Convective Heating Environments for Materials Evaluation. General Electric Co., MSD TIS R64 SD 24, Mar. 1964.
8. Roberts, L.: Ablation Materials for Atmospheric Entry. Proceedings of the NASA-University Conference on the Science and Technology of Space Exploration, Chicago, Illinois, Nov. 1-3, NASA SP-11, vol. 2, pp. 461-467.
9. Dow, M. B.: Comparison of Measurements of Internal Temperatures in Ablation Material by Various Thermocouple Configurations. NASA TN D-2165, 1964.
10. Peters, R. W.; and Wilson, R. G.: Experimental Investigation of the Effect of Convective and Radiative Heat Loads on the Performance of Subliming and Charring Ablators. NASA TN D-1355, 1962.
11. Swann, R. T.: Effect of Thermal Radiation From a Hot Gas Layer on Heat of Ablation. Journal of Aerospace Sciences (Readers' Forum), vol. 25, no. 7, July 1961, pp. 582-583.
12. Dow, M. B.; and Swann, R. T.: Determination of Effects of Oxidation on Performance of Charring Ablators. NASA TR R-196, 1964.

13. Clark, R. K.: Effect of Environmental Parameters on the Performance of Low-Density Silicone-Resin and Phenolic-Nylon Ablation Materials. NASA TN D-2543, 1965.
14. Swann, R. T.; Dow, M. B.; and Tompkins, S. S.: Analysis of the Effects of Environmental Conditions on the Performance of Charring Ablators. Presented at the AIAA Entry Technology Conference, Williamsburg and Hampton, Virginia, Oct. 12-14, 1964.



NASA

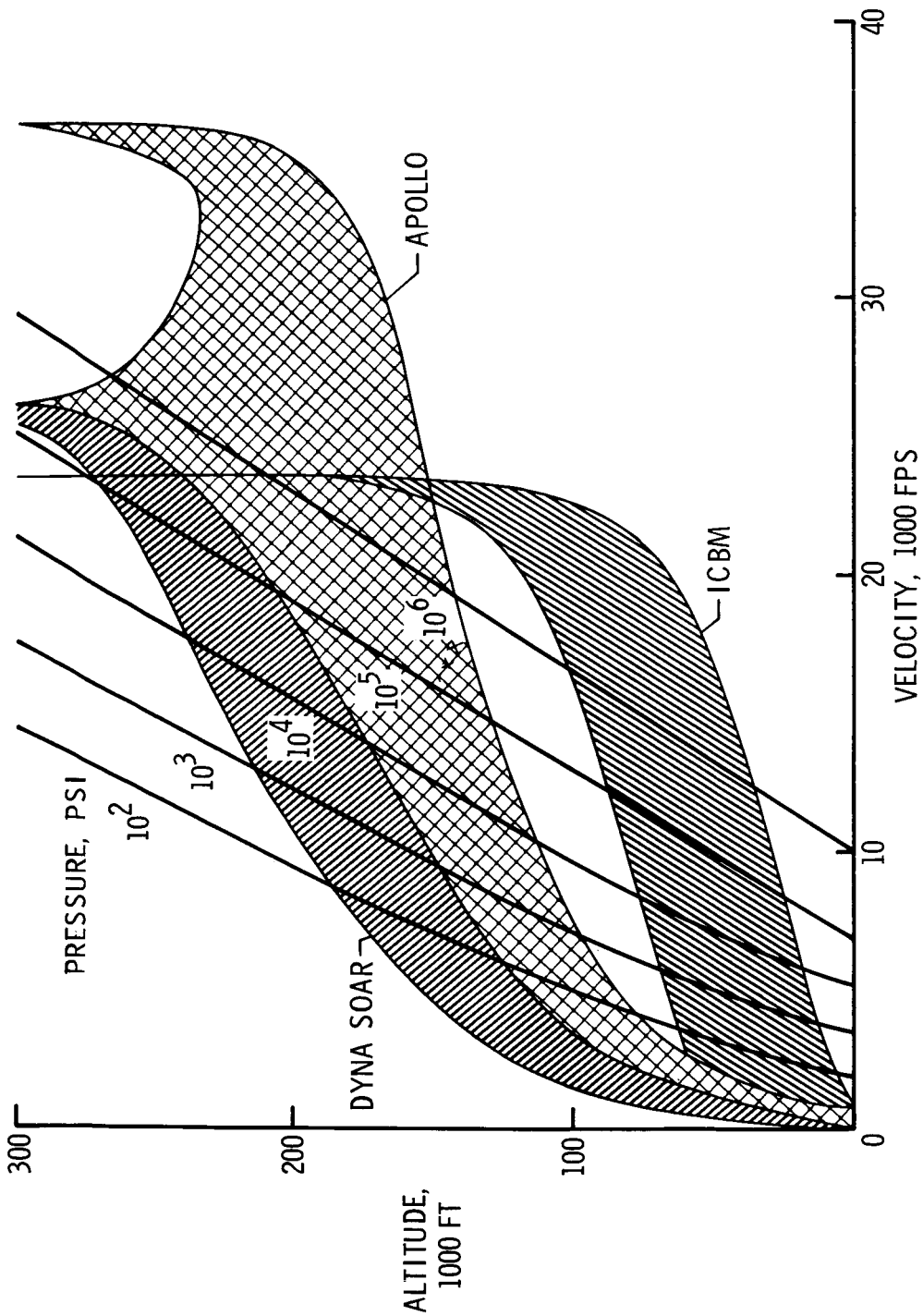
Figure 1.- Dissipation of the kinetic energy of entry vehicles.



NASA

Figure 2.- Entry vehicle flight regions.

EXACT FLOW DUPLICATION



NASA

Figure 3.- Settling chamber pressure required for exact flow duplication.

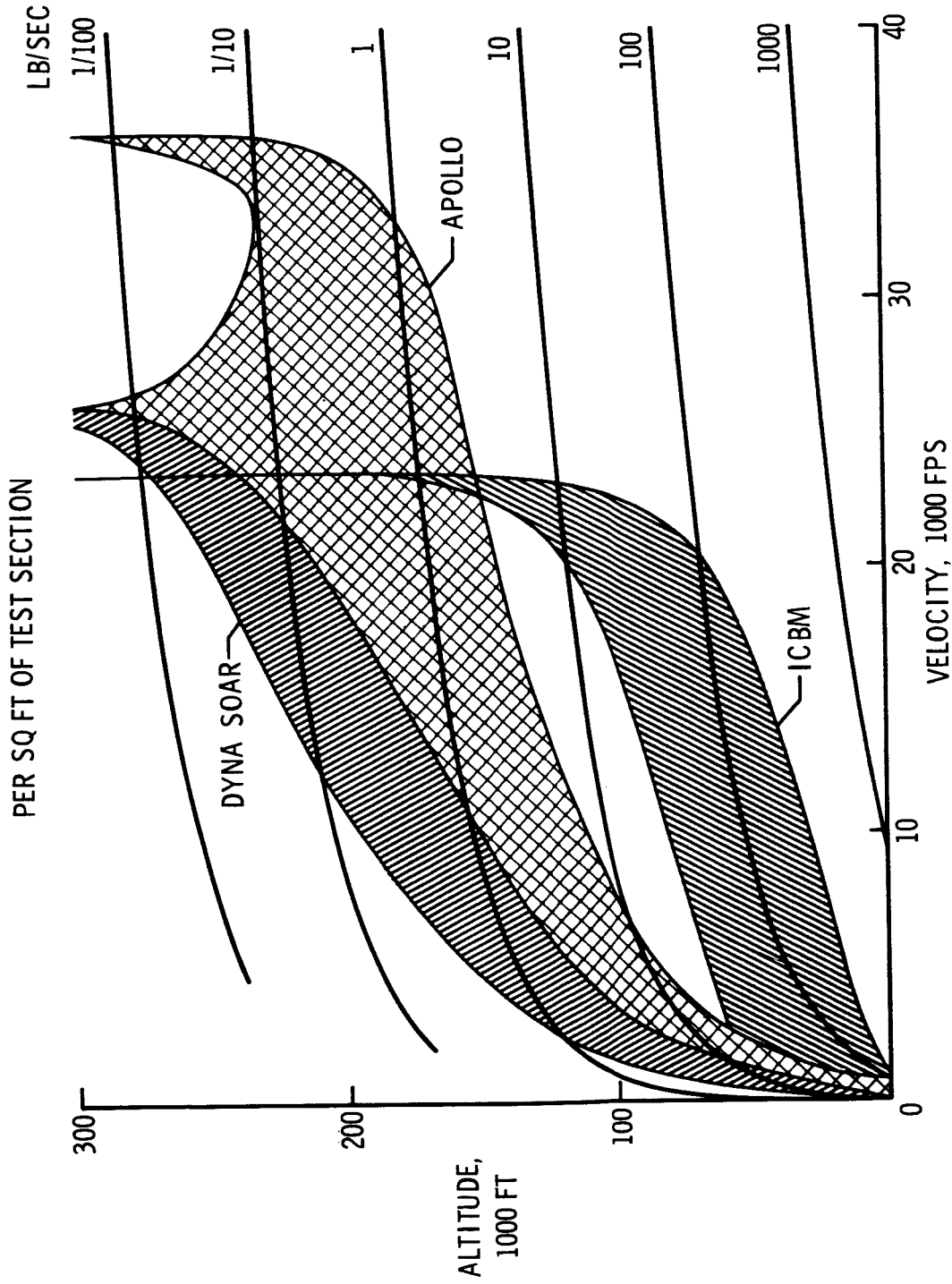


Figure 4.- Mass flow rate required for exact flow duplication.

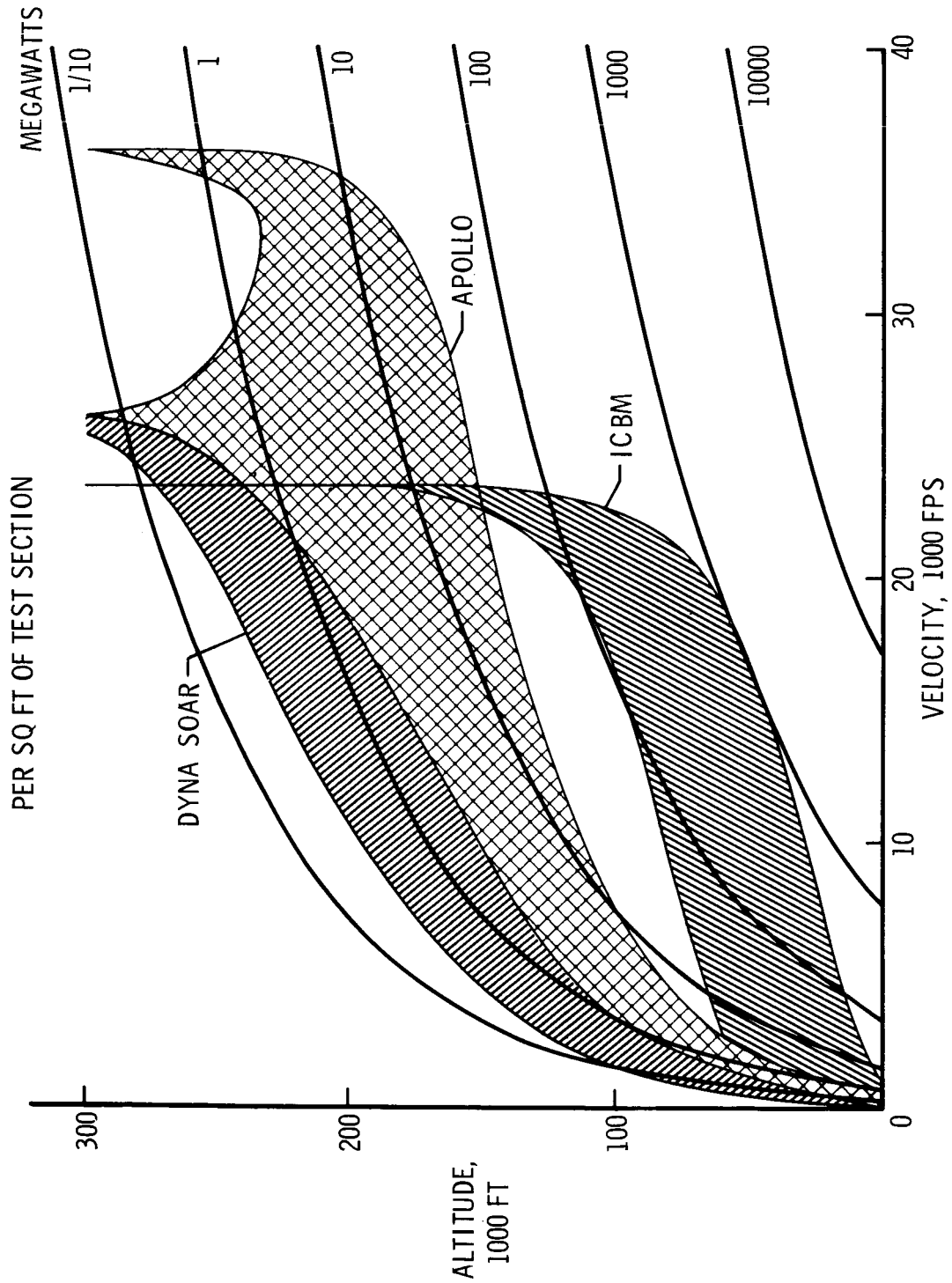
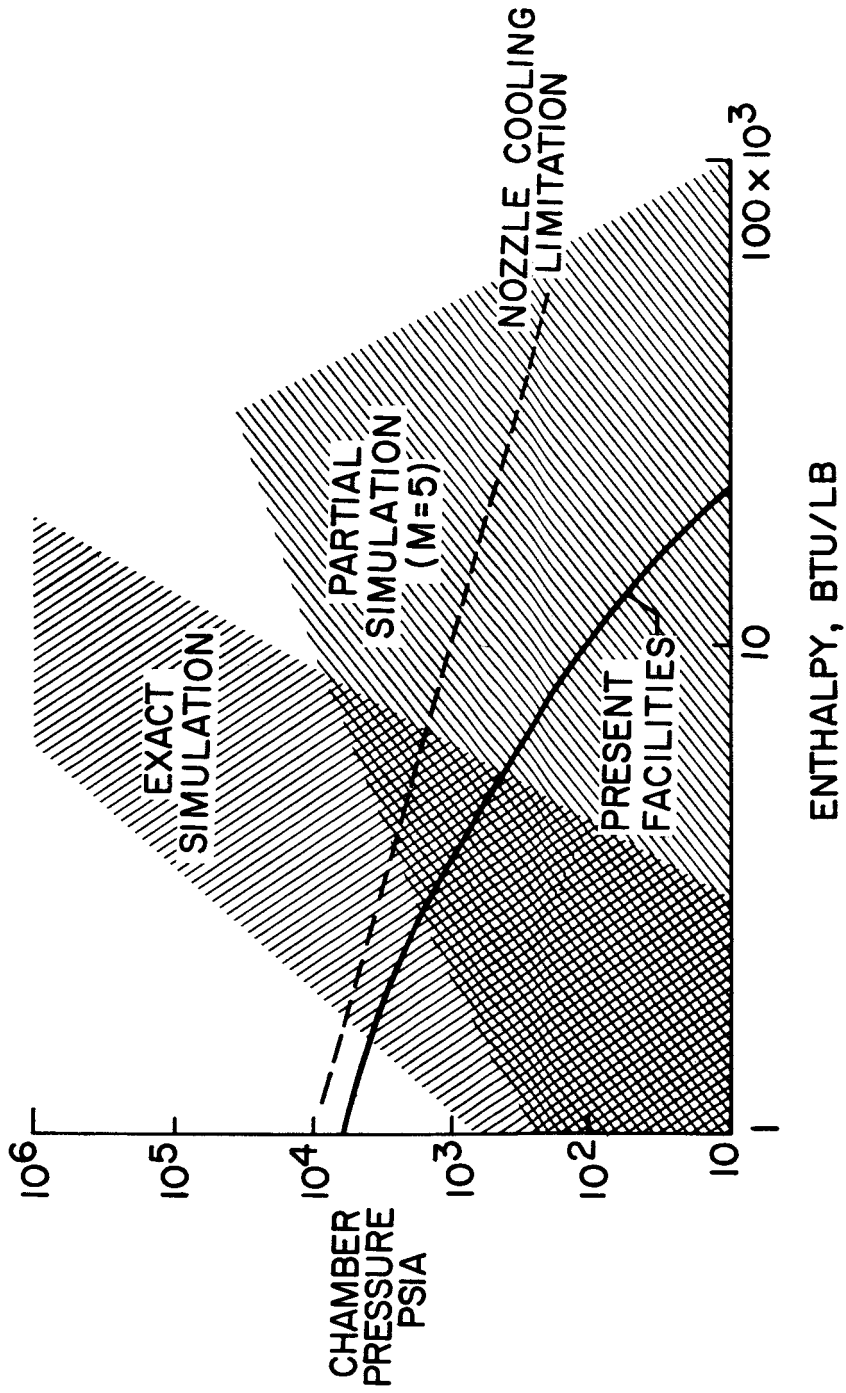
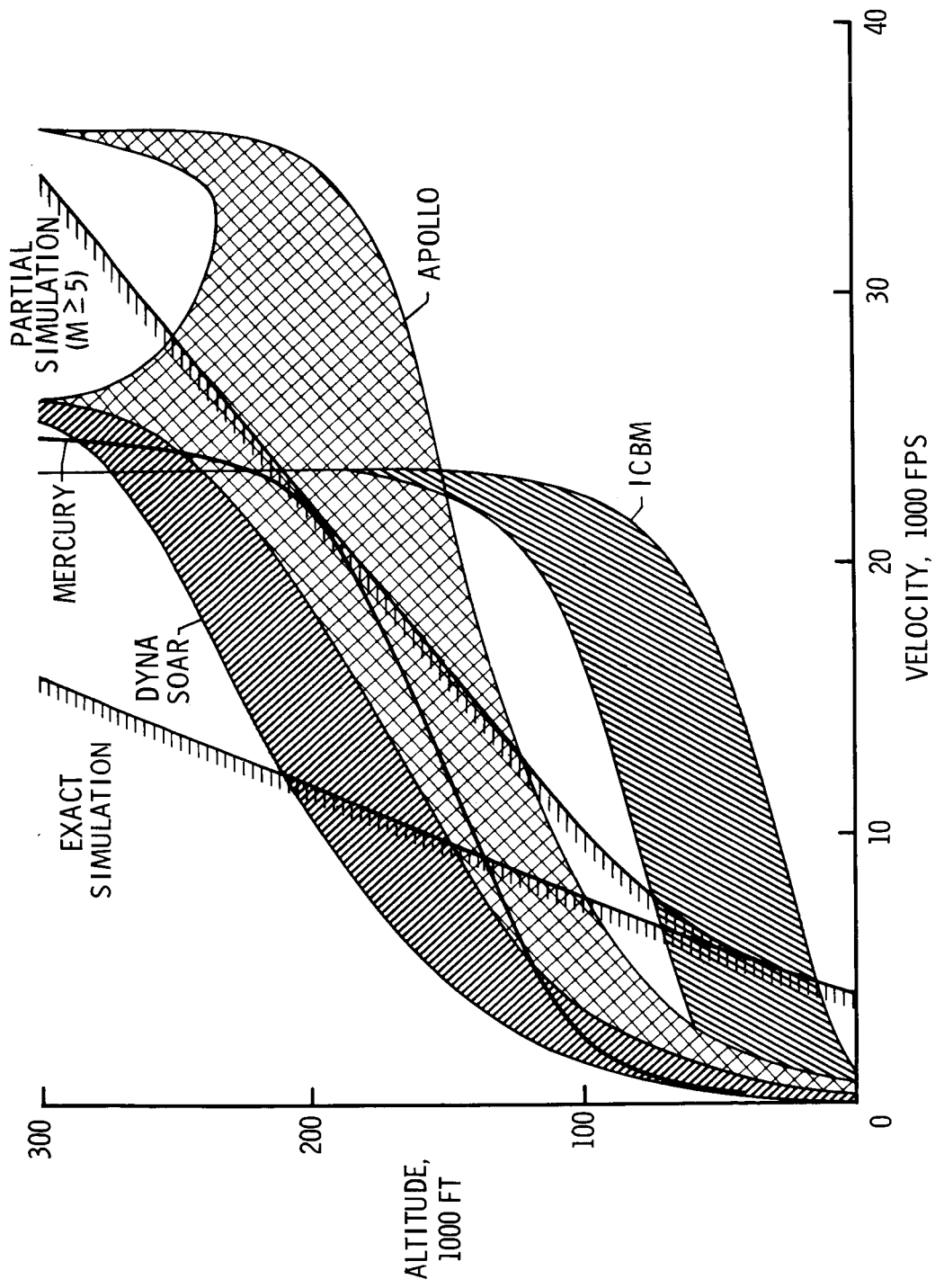


Figure 5.- Heat energy required for exact flow duplication.



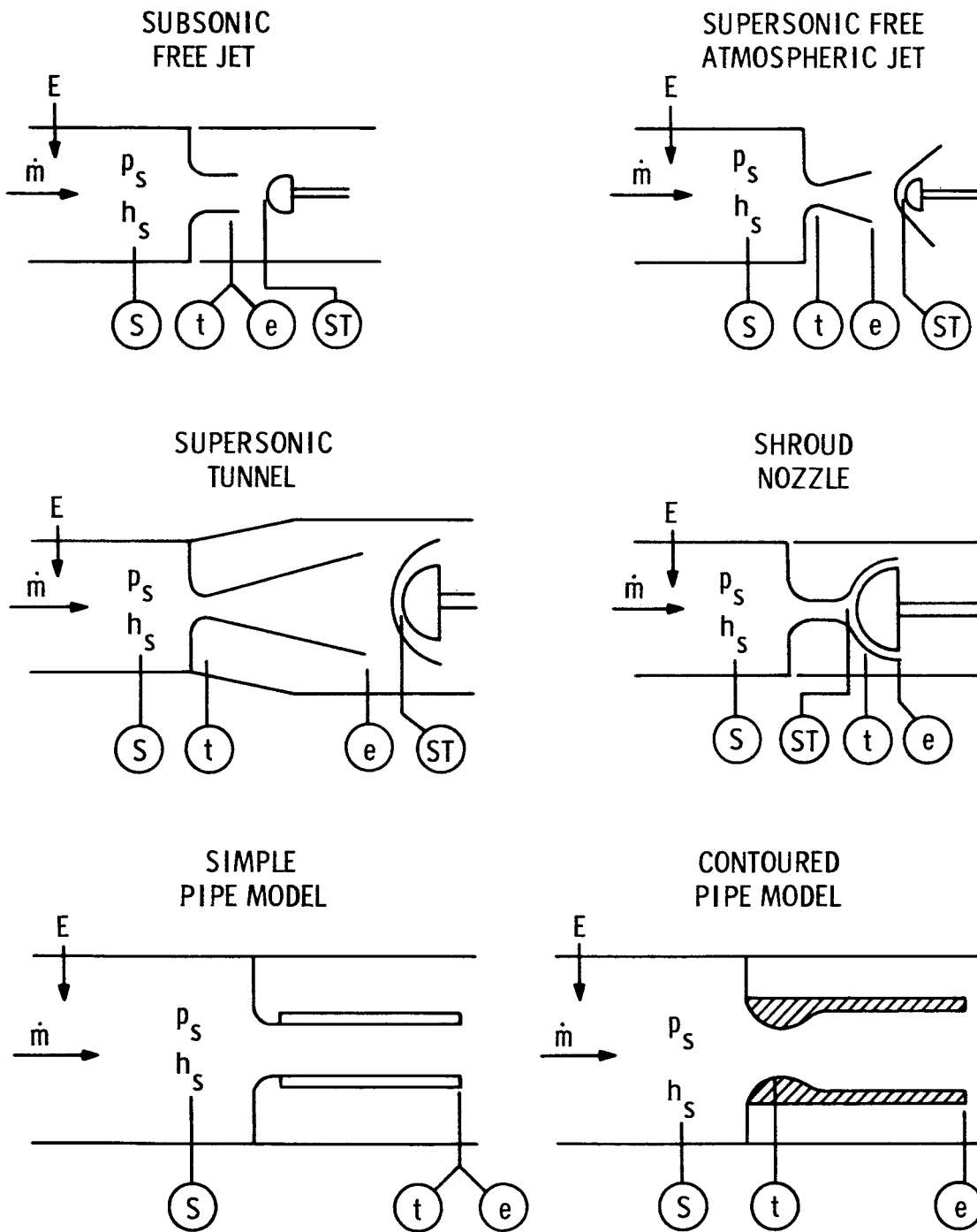
NASA

Figure 6.- Capabilities of present arc facilities.



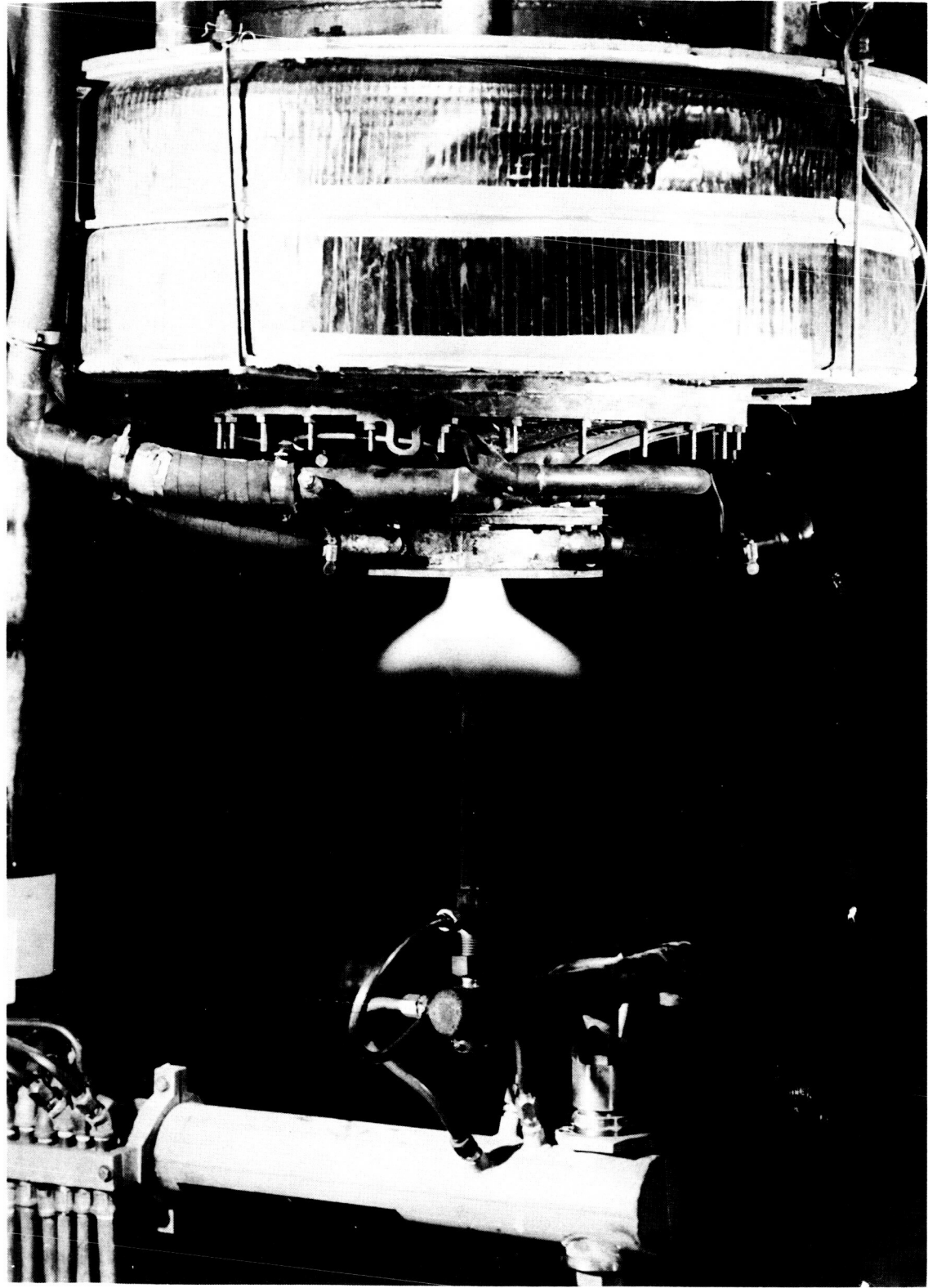
NASA

Figure 7.- Comparison of arc facilities simulation capabilities with entry flight regions.



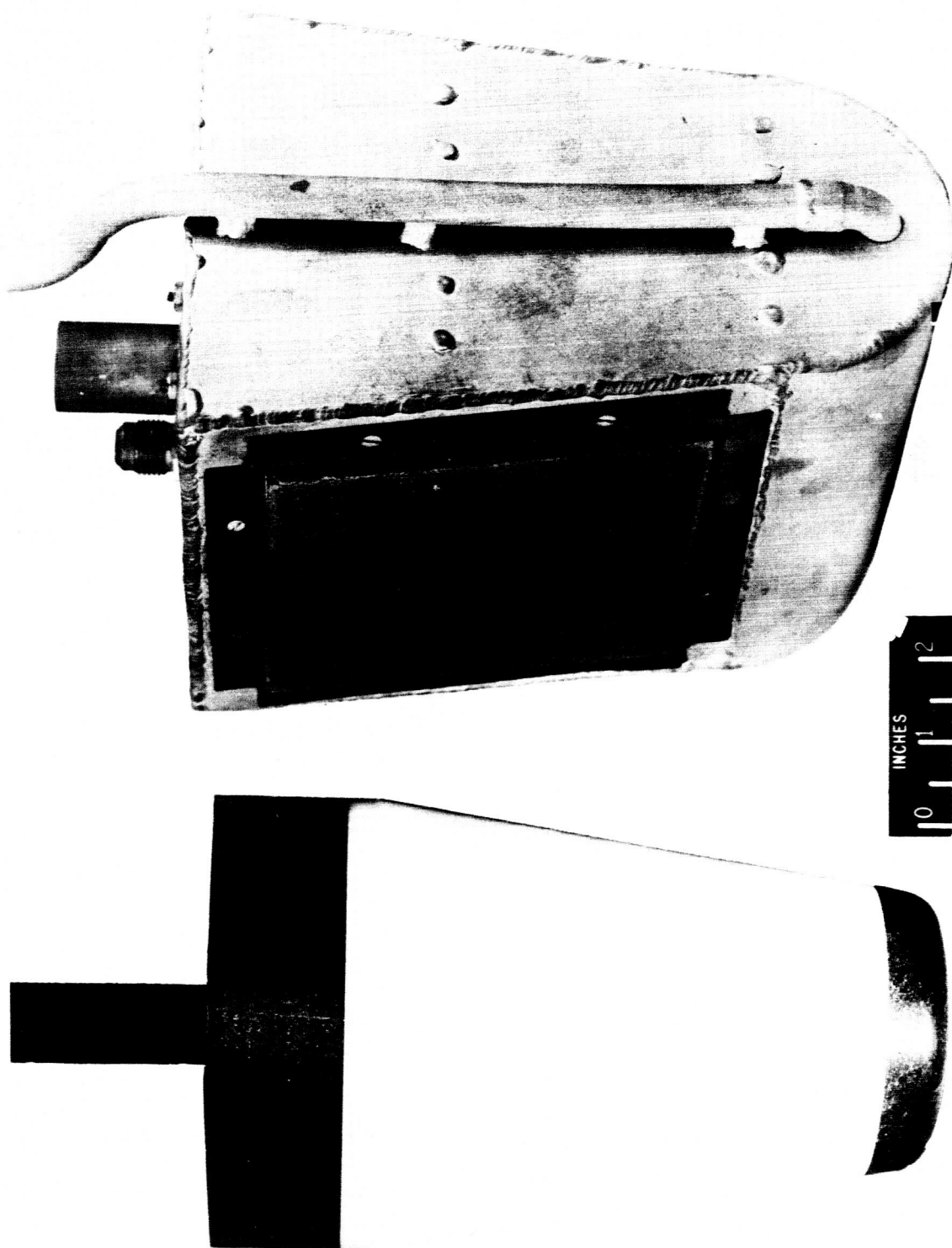
NASA

Figure 8.- Configurations of test streams produced by arc facilities.



NASA

Figure 9.- A splash test in the Langley Research Center 2500-kilowatt arc jet.



NASA

Figure 10.- Configuration of test specimens.

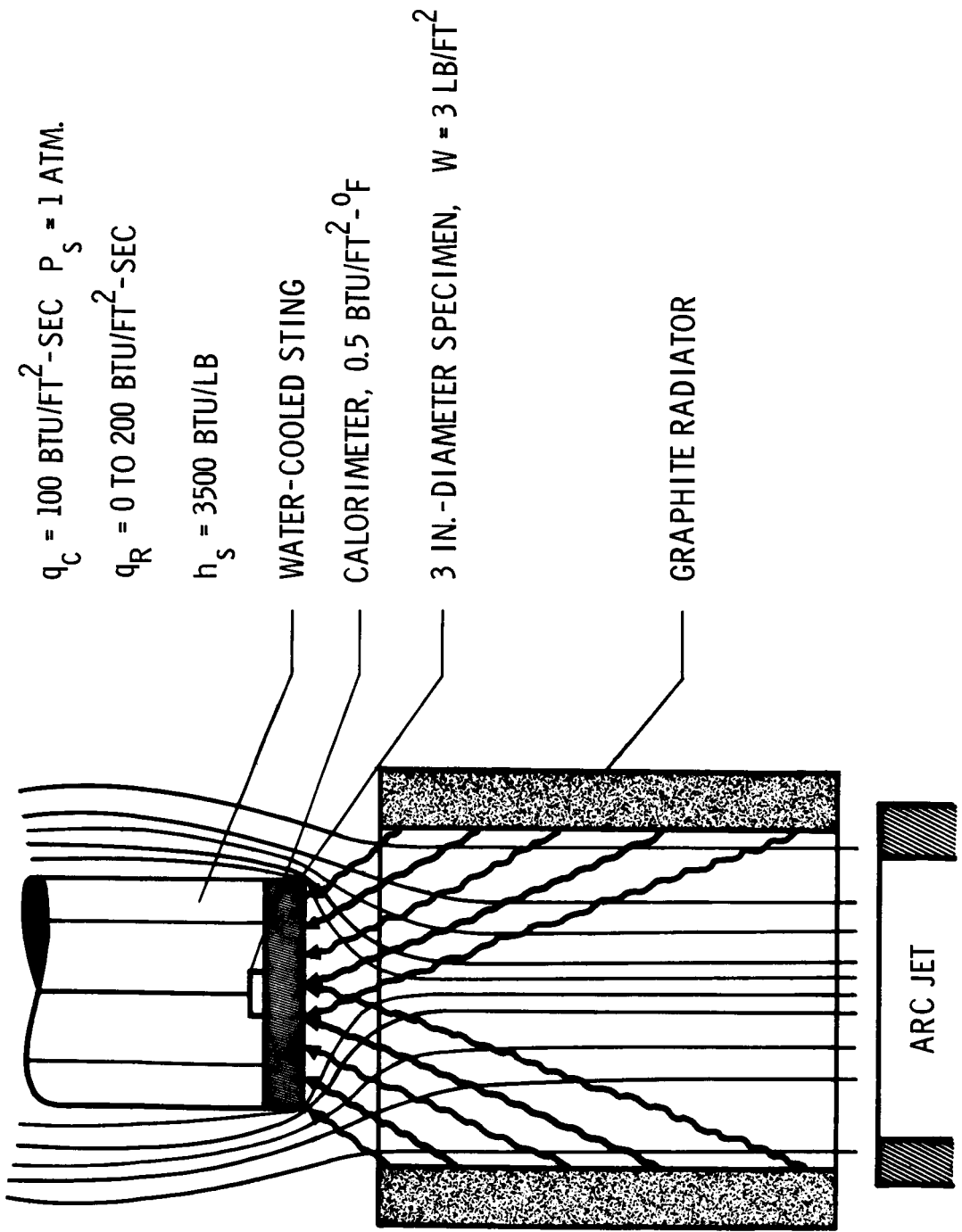
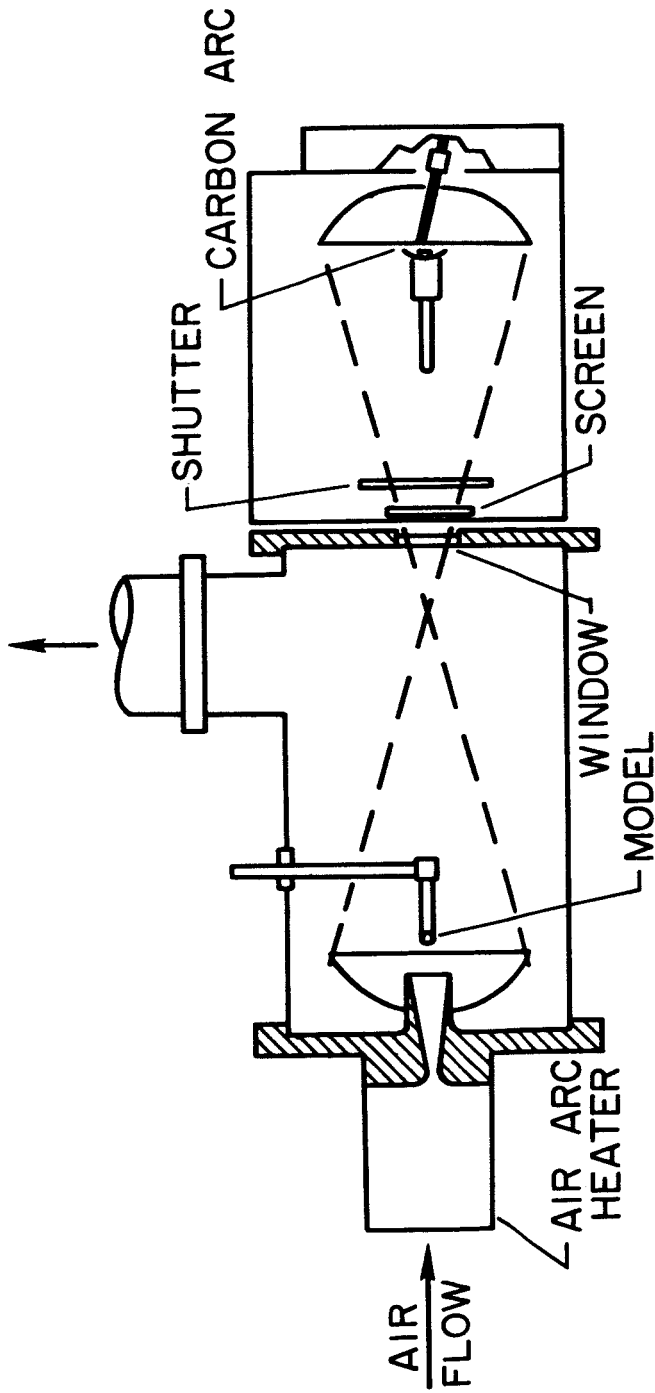


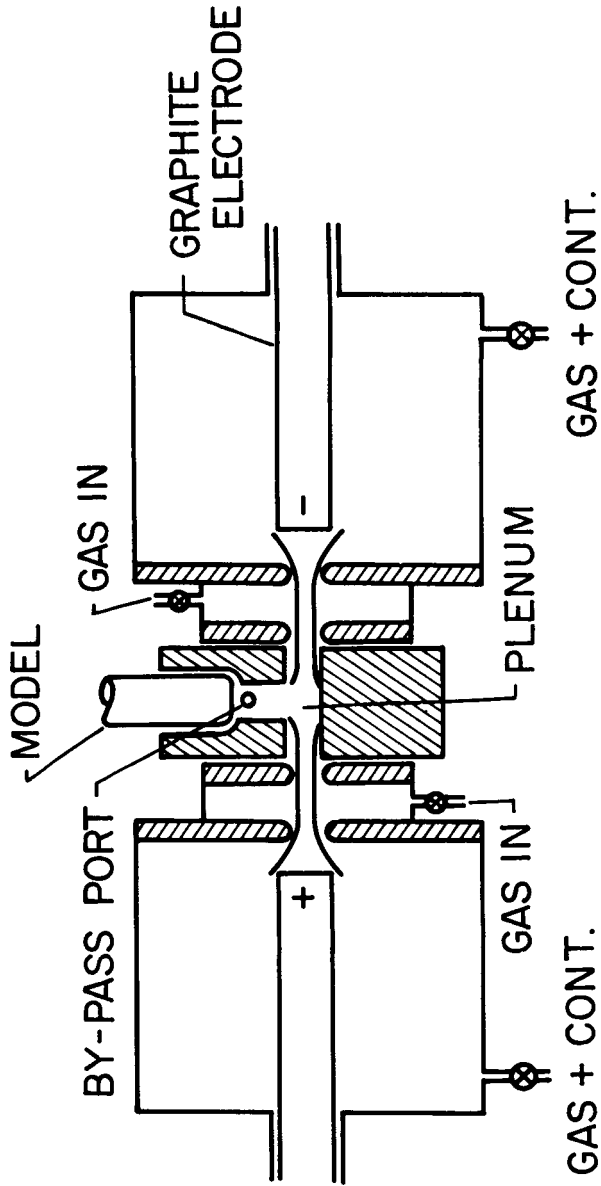
Figure 11.- Convective and radiative heating device used at Langley Research Center.



MODEL DIAMETER = 0.75 IN.  
 CONVECTIVE HEATING RATE = 600 BTU/FT<sup>2</sup>-SEC  
 RADIATIVE HEATING RATE = 750 BTU/FT<sup>2</sup>-SEC

NASA

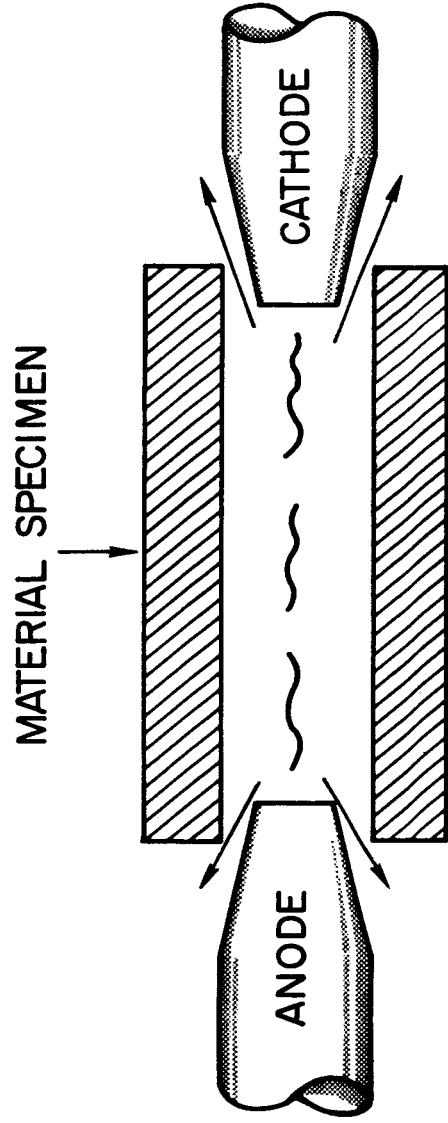
Figure 12.- The Ames Research Center Entry Heating Simulator.



MODEL DIAMETER = 0.75 IN.  
 CONVECTIVE HEATING RATE = 0-2000 BTU/FT<sup>2</sup> - SEC  
 RADIATIVE HEATING RATE = 0-500 BTU/FT<sup>2</sup> - SEC

NASA

Figure 13.- General Electric Company's tandem Gerdien arc.



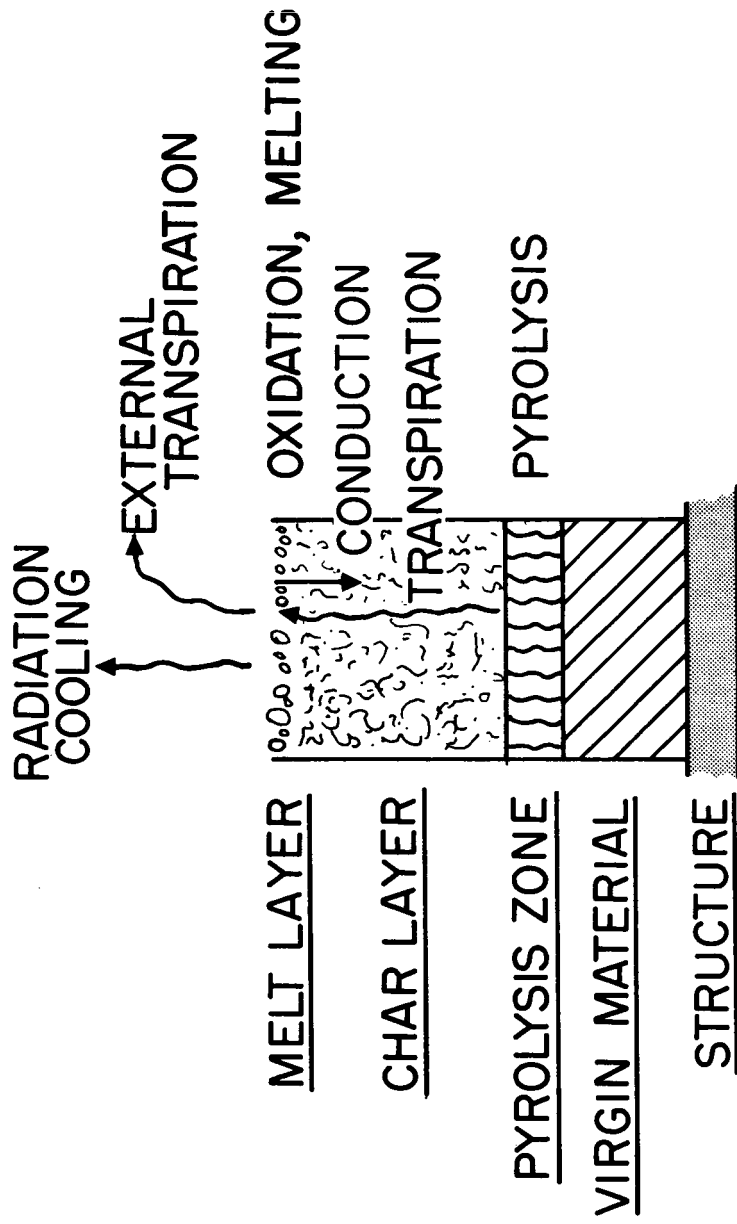
SPECIMEN INSIDE DIAMETER = 1.2 IN.

RADIATIVE HEATING RATE = 45,000 BTU/FT<sup>2</sup> - SEC

NASA

Figure 14.- A radiative heating device wherein the test material contains the electric arc.

*PHENOLIC-NYLON; PHENOLIC-ASBESTOS; PHENOLIC-GLASS*



NASA

Figure 15.- The zones and functions of a charring ablator.

SURFACE ENERGY BALANCE:

$$q_c \left( 1 - \frac{h_w}{h_e} \right) \left[ \dot{m}_T \frac{h_e}{q_c} \right] + \alpha q_R + \dot{m}_c \Delta h_c$$

NET CONVECTIVE HEATING

RADIATIVE HEATING + COMBUSTIVE HEATING

$$= \sigma \epsilon_1 T_1^4 - k \frac{\partial T}{\partial x} + \dot{m}_c H_c$$

RERRADIATION CONDUCTION TO INTERIOR + HEAT OF SUBLIMATION

DEGRADING MATERIAL ENERGY BALANCE:

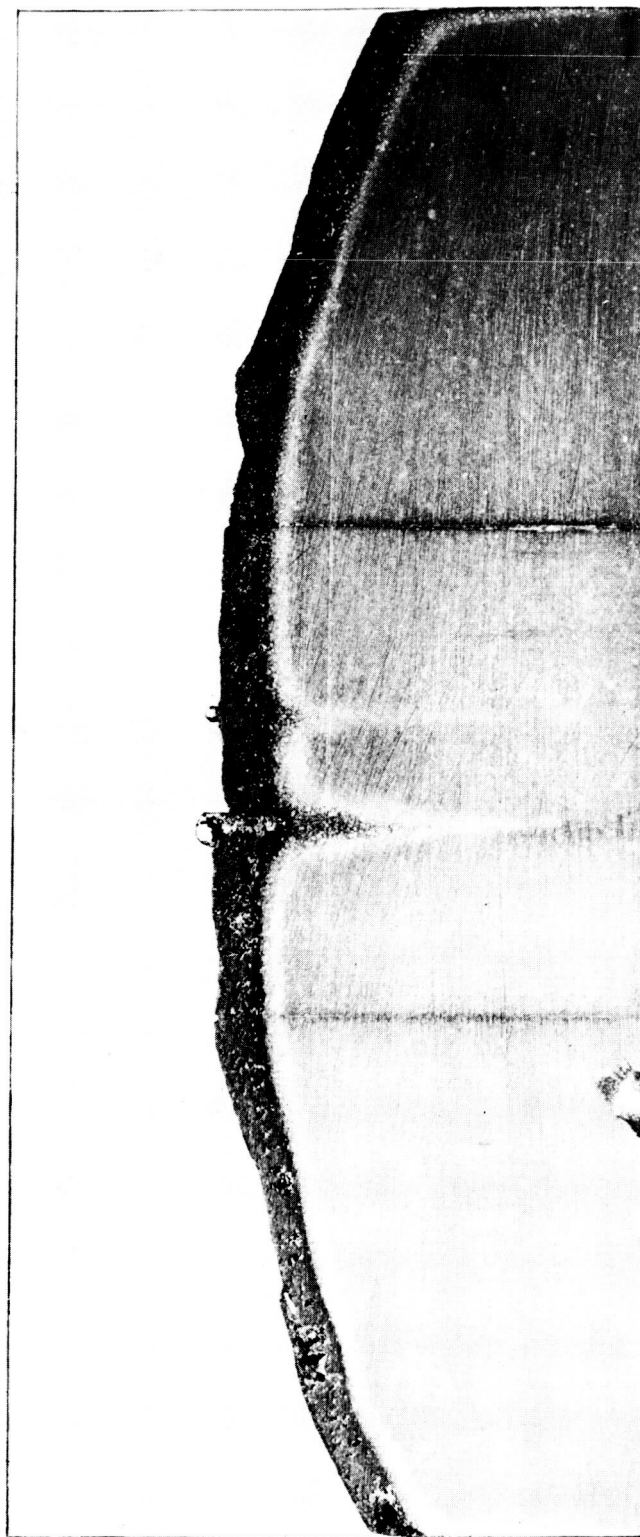
$$\frac{\partial}{\partial x} \left( k \frac{\partial T}{\partial x} \right) + \frac{\partial}{\partial x} \left[ \sum \dot{m}_i h_i \right] = \frac{\partial}{\partial t} \left[ \sum \rho_j h_j \right]$$

HEAT CONDUCTED + HEAT CONVECTED = HEAT ABSORBED

NASA

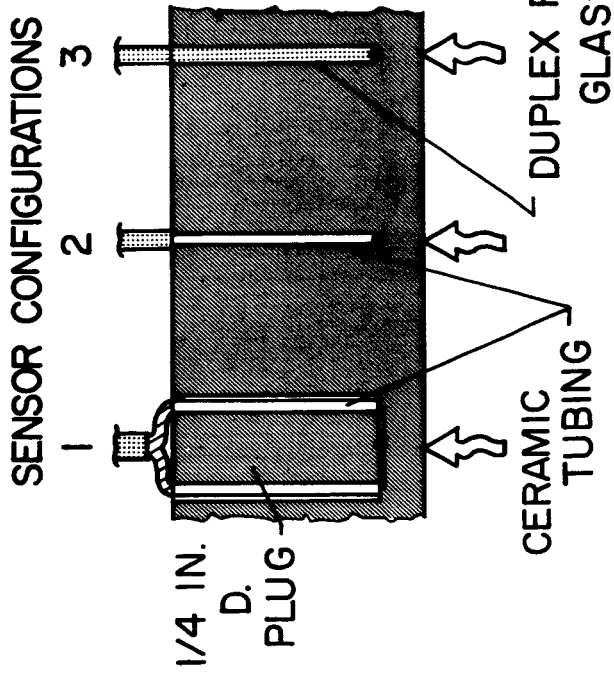
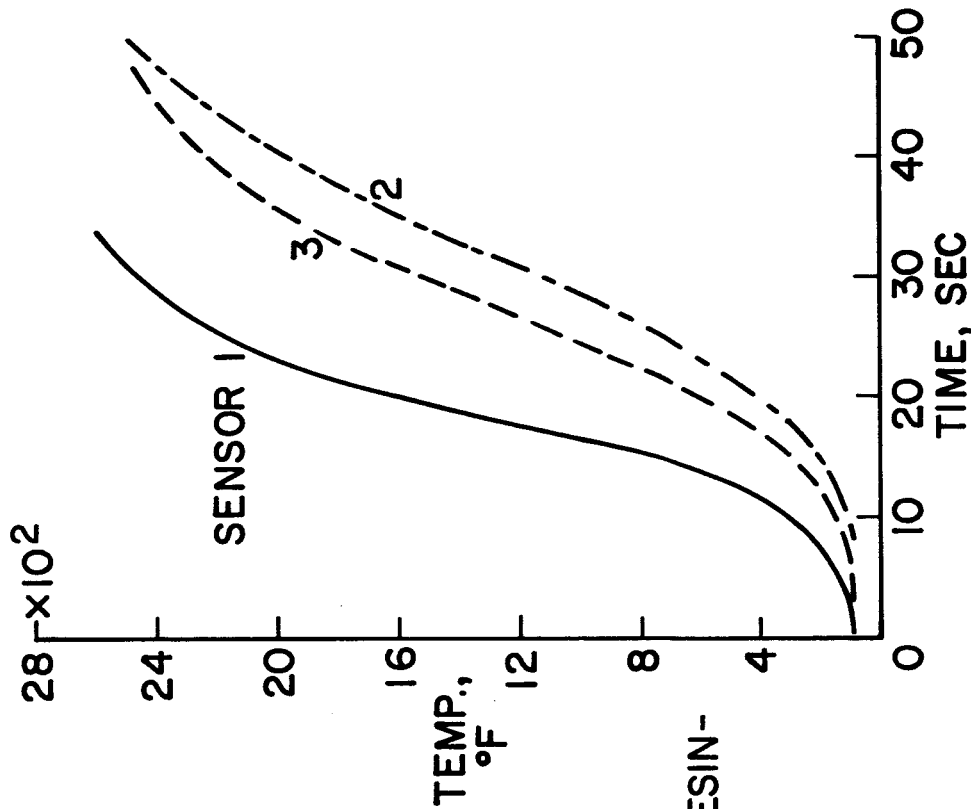
Figure 16.- The basic equations for ablation.

PHENOLIC-NYLON 76 LB/FT<sup>3</sup>  
PT-PT 13% RH TC, # 24 AND # 30  
 $\dot{q} = 90 \text{ BTU/FT}^2 - \text{SEC}$ ,  $t = 135 \text{ SEC}$



NASA

Figure 17.- The conduction of heat along thermocouple wire.



NASA

Figure 18.- The effect of thermocouple configuration on temperature measure.

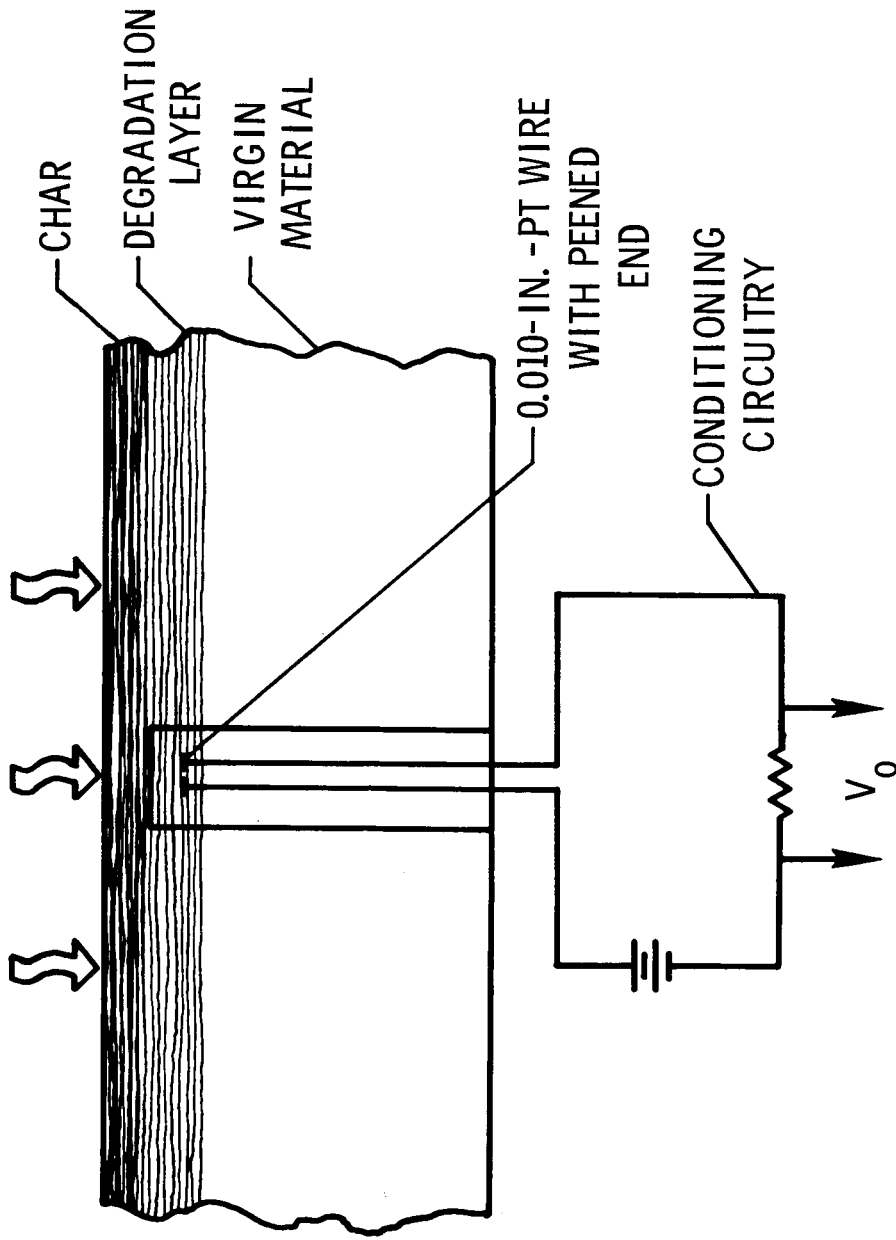


Figure 19.- The make-wire ablation sensor.

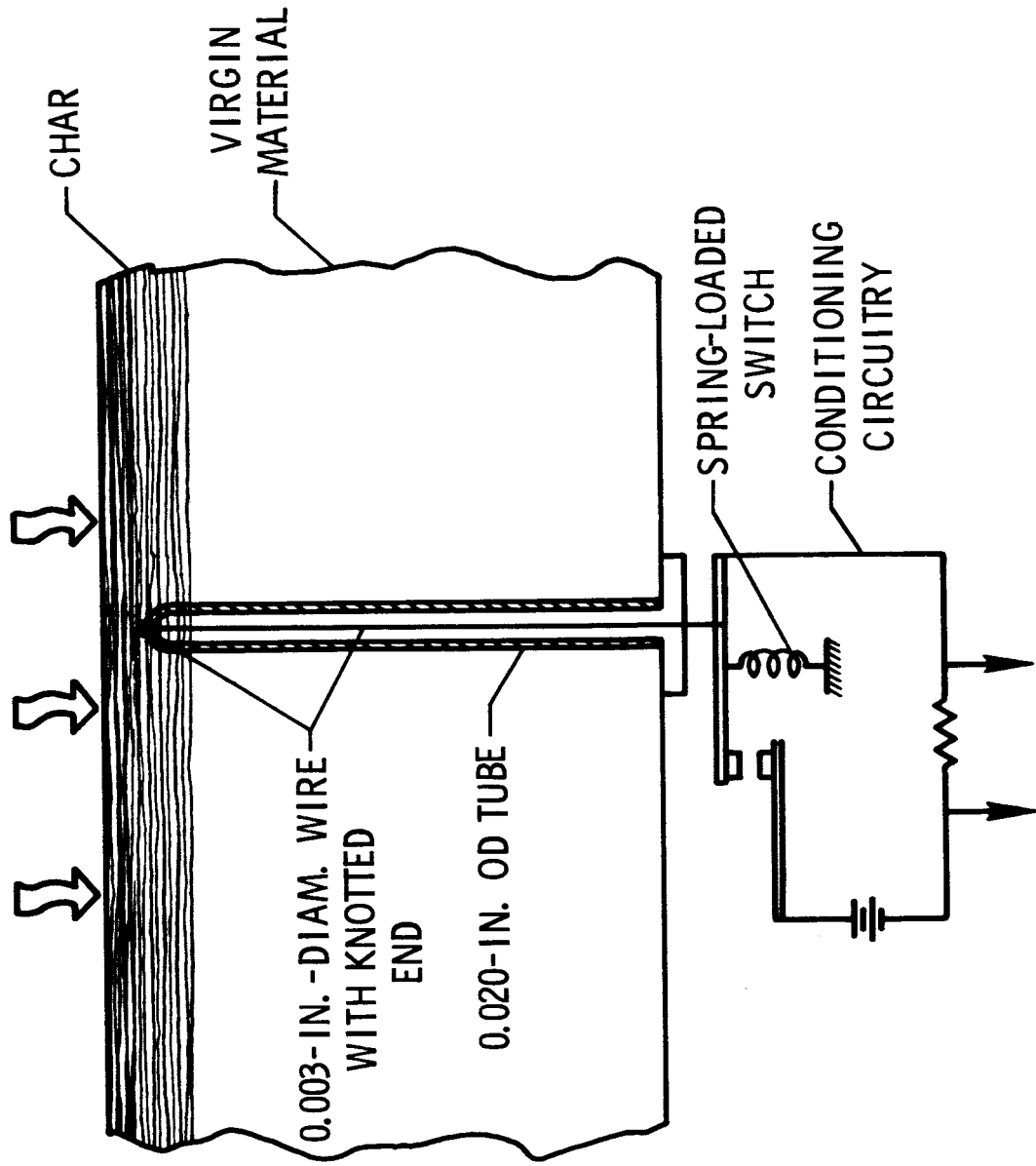
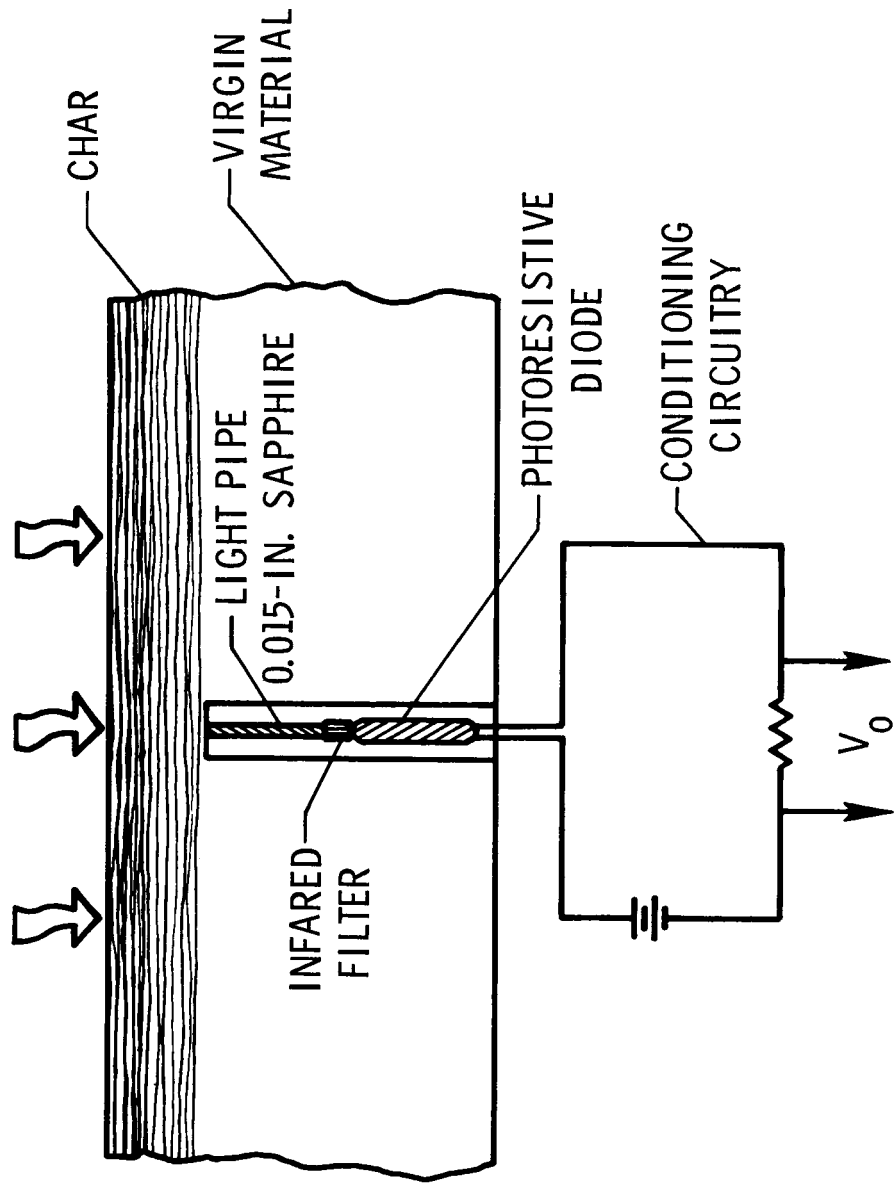


Figure 20.- The spring-wire ablation sensor.



NASA

Figure 21.- The light-pipe ablation sensor.

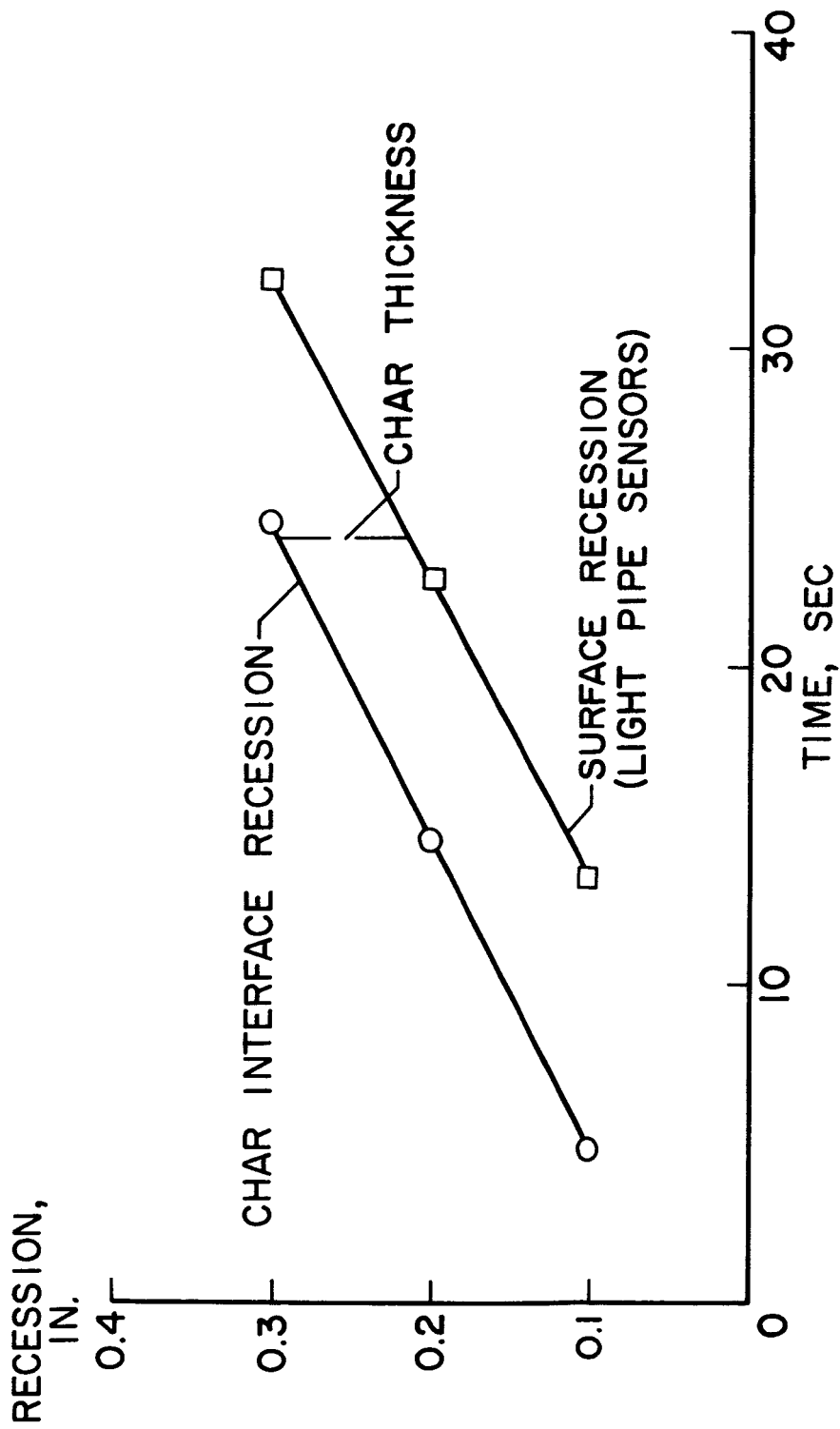
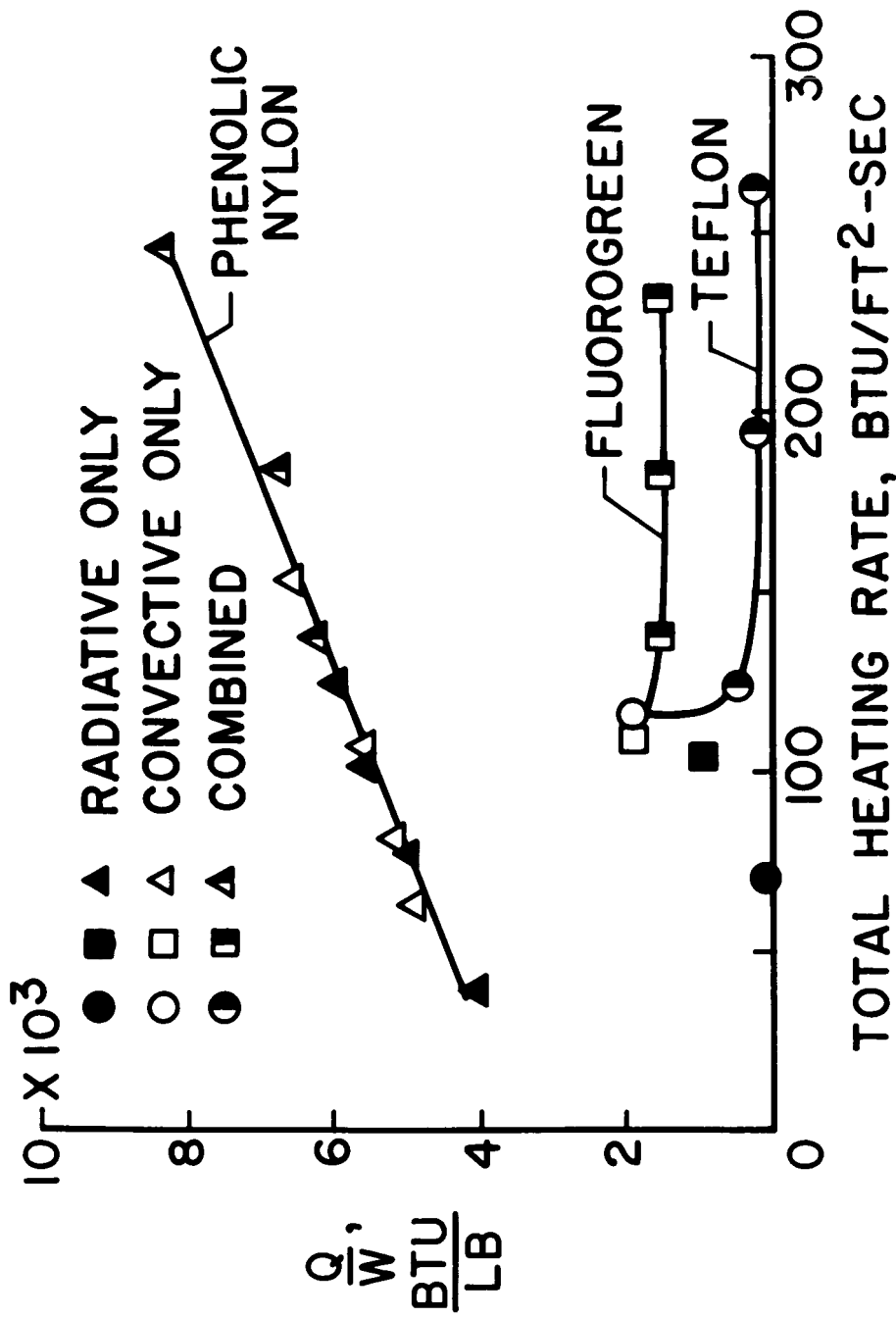


Figure 22.- Determination of char thickness with ablation sensors.

BACK SURFACE TEMPERATURE RISE = 300 °F; W = 3 LB/FT<sup>2</sup>



NASA

Figure 23.- The effect of radiative heating on ablation material performance.

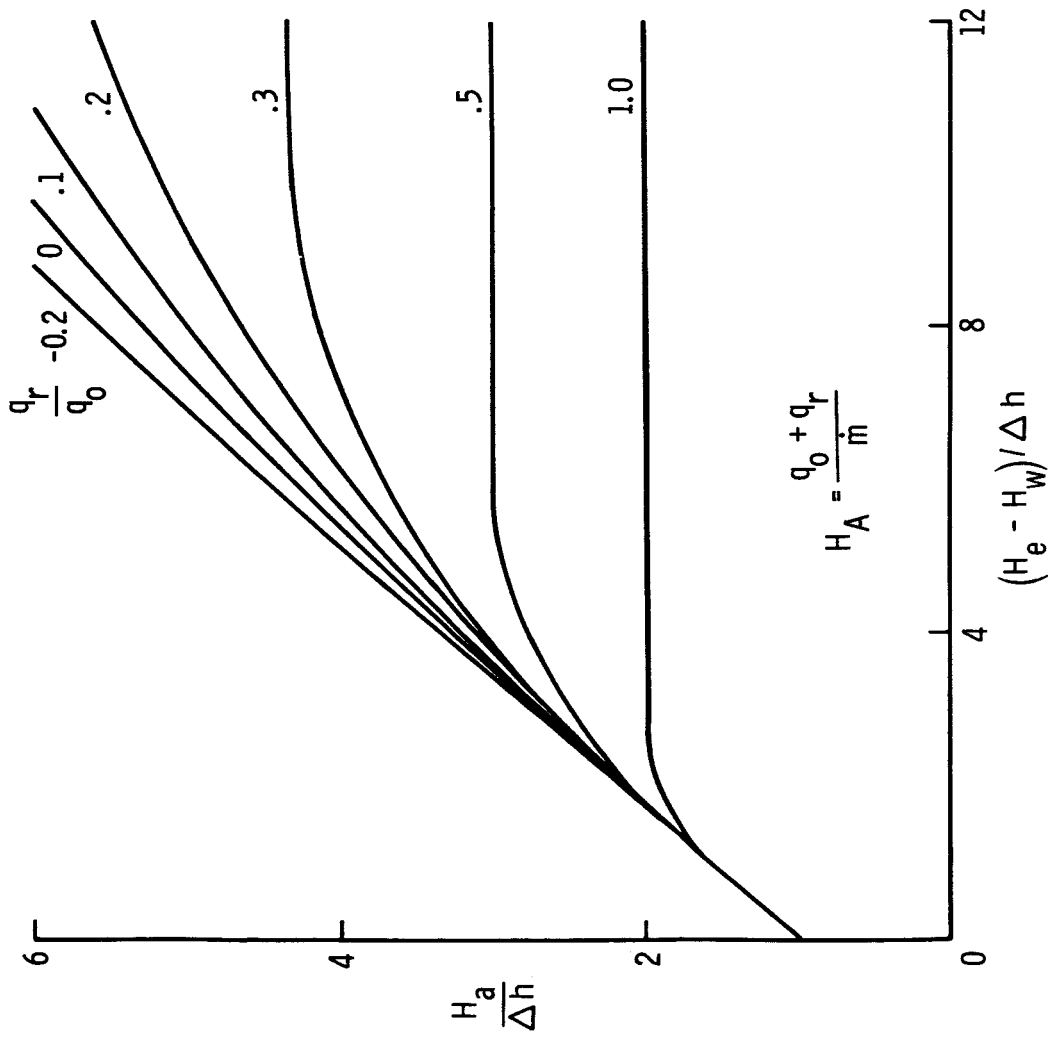


Figure 24.- Calculated ablation efficiency with radiative heating.

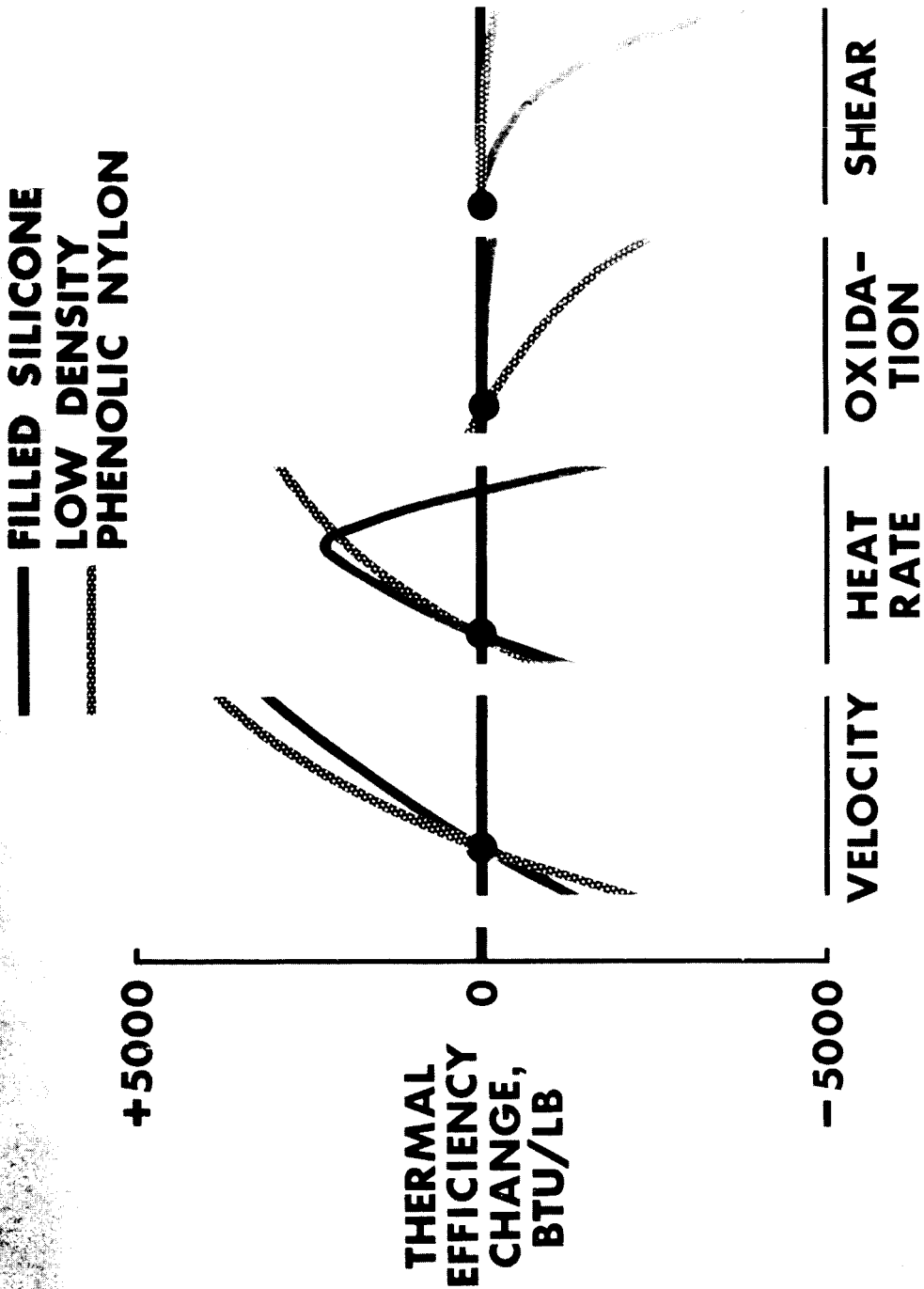


Figure 25.- The effect of environmental parameters on heat-shield efficiency.

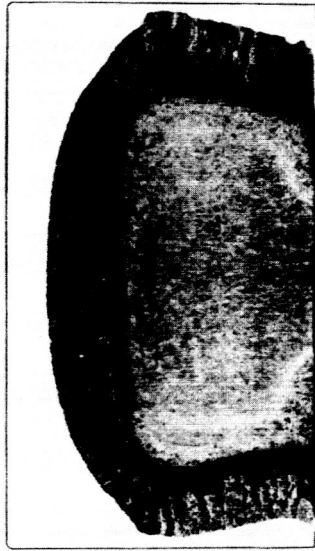
PHENOLIC-NYLON,  $W=9 \text{ LB/FT}^2$

$q_c = 110 \text{ BTU/FT}^2\text{-SEC}$

5 MINUTE EXPOSURE



100 % N<sub>2</sub>



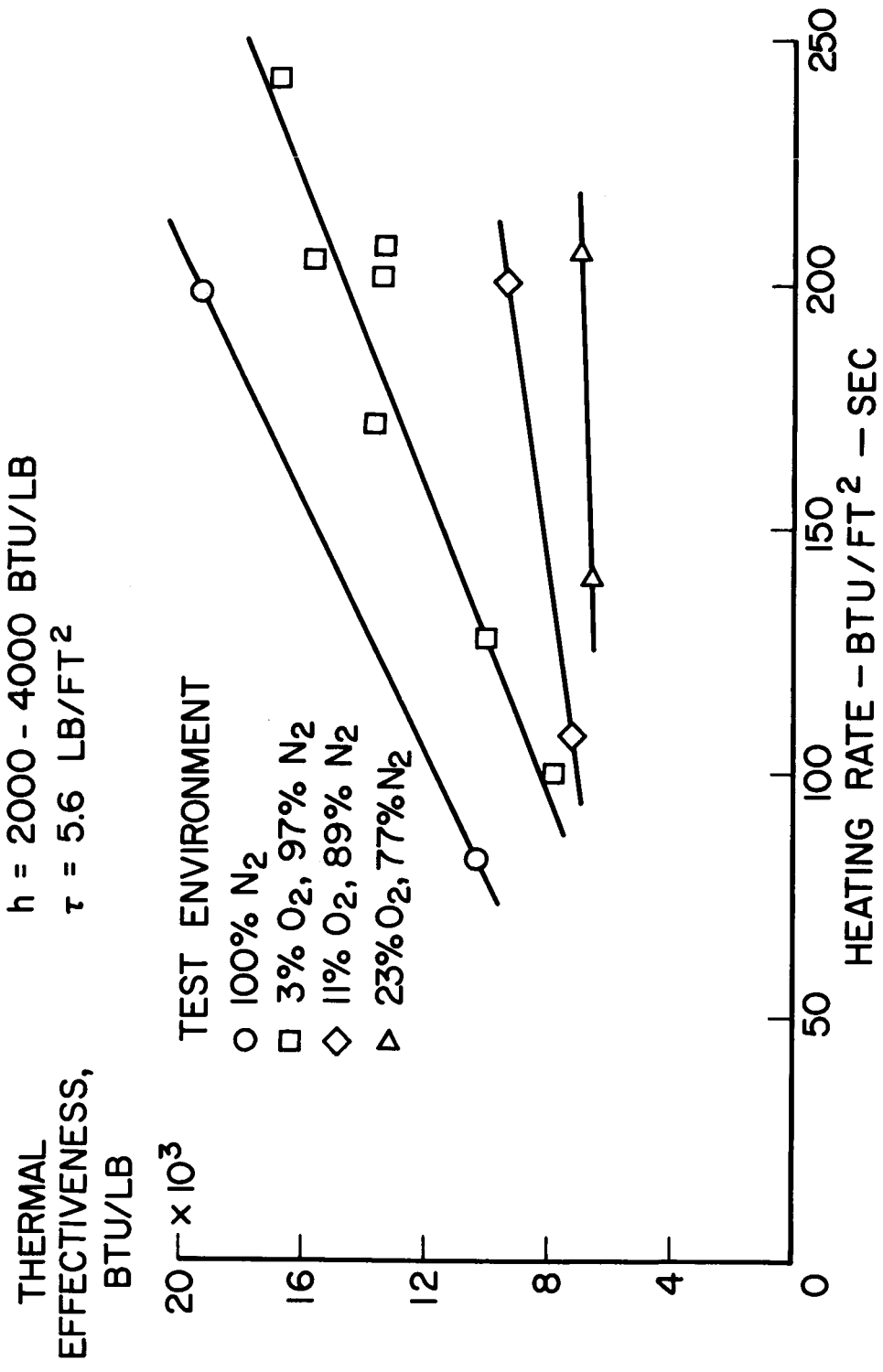
90% N<sub>2</sub> + 10% O<sub>2</sub>



AIR

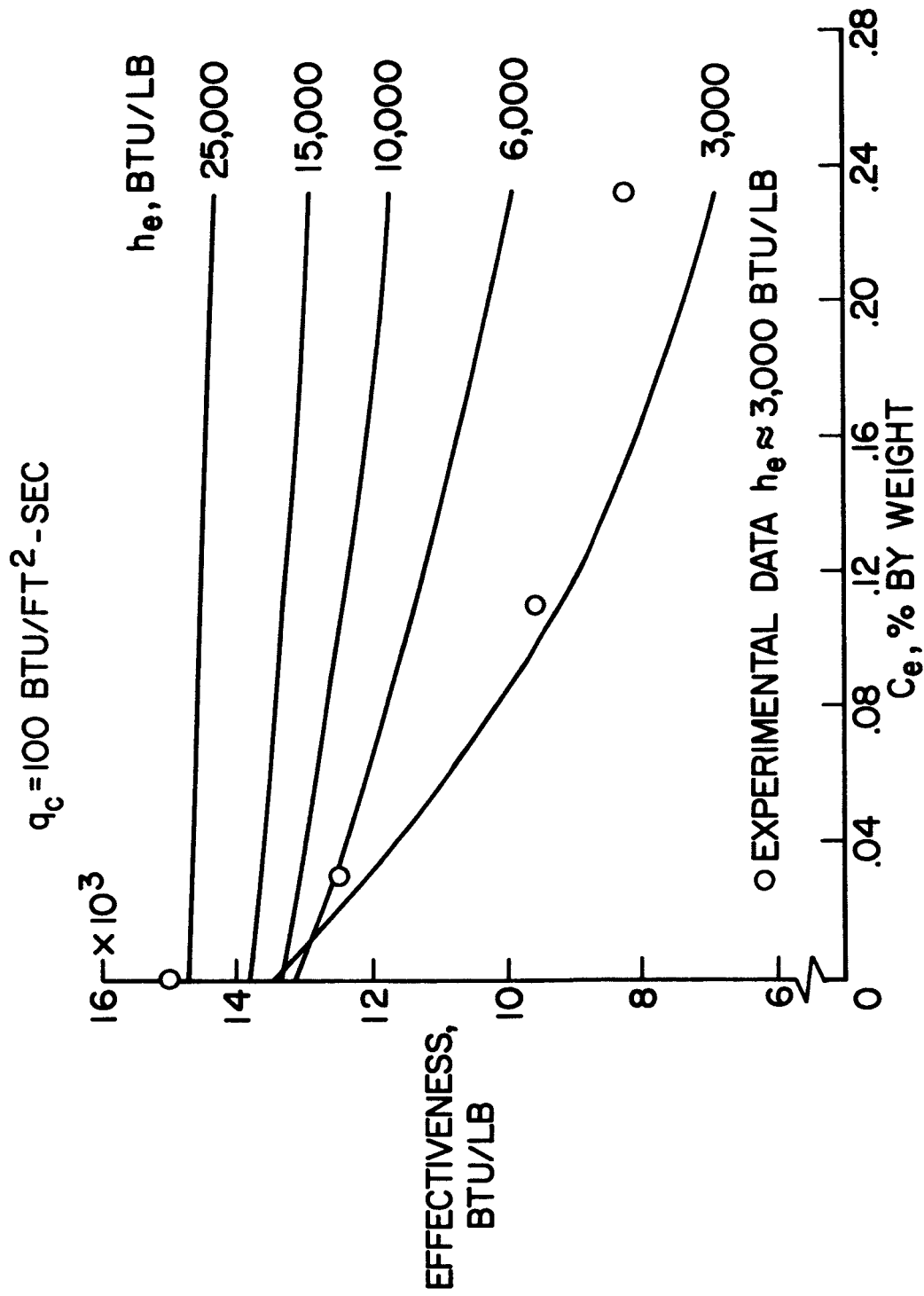
NASA

Figure 26.- The effect of oxygen on char erosion.



NASA

Figure 27.- The thermal effectiveness of low-density phenolic-nylon in various gas streams.



NASA

Figure 28.- The effect of oxidation on the efficiency of a charring ablator.

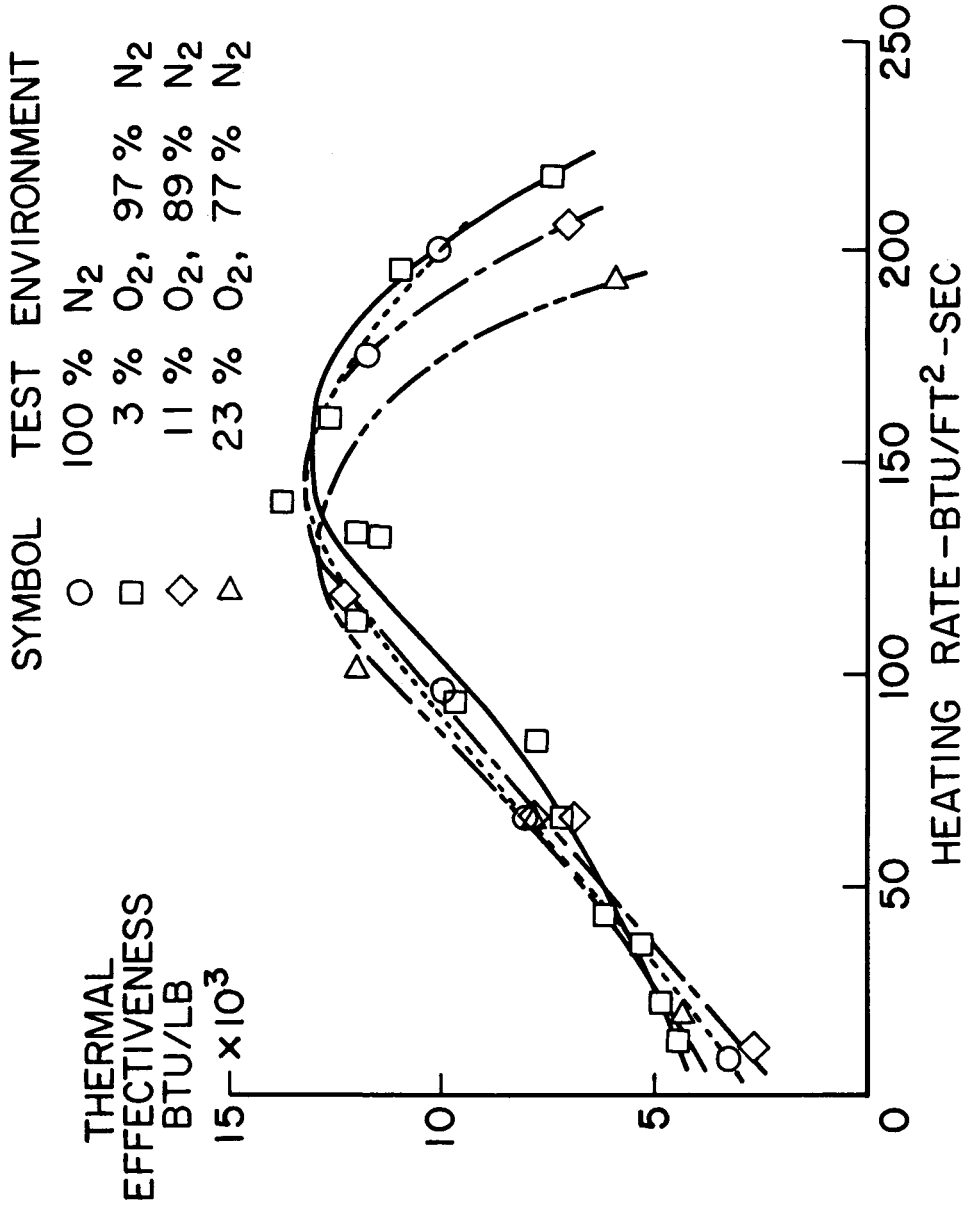
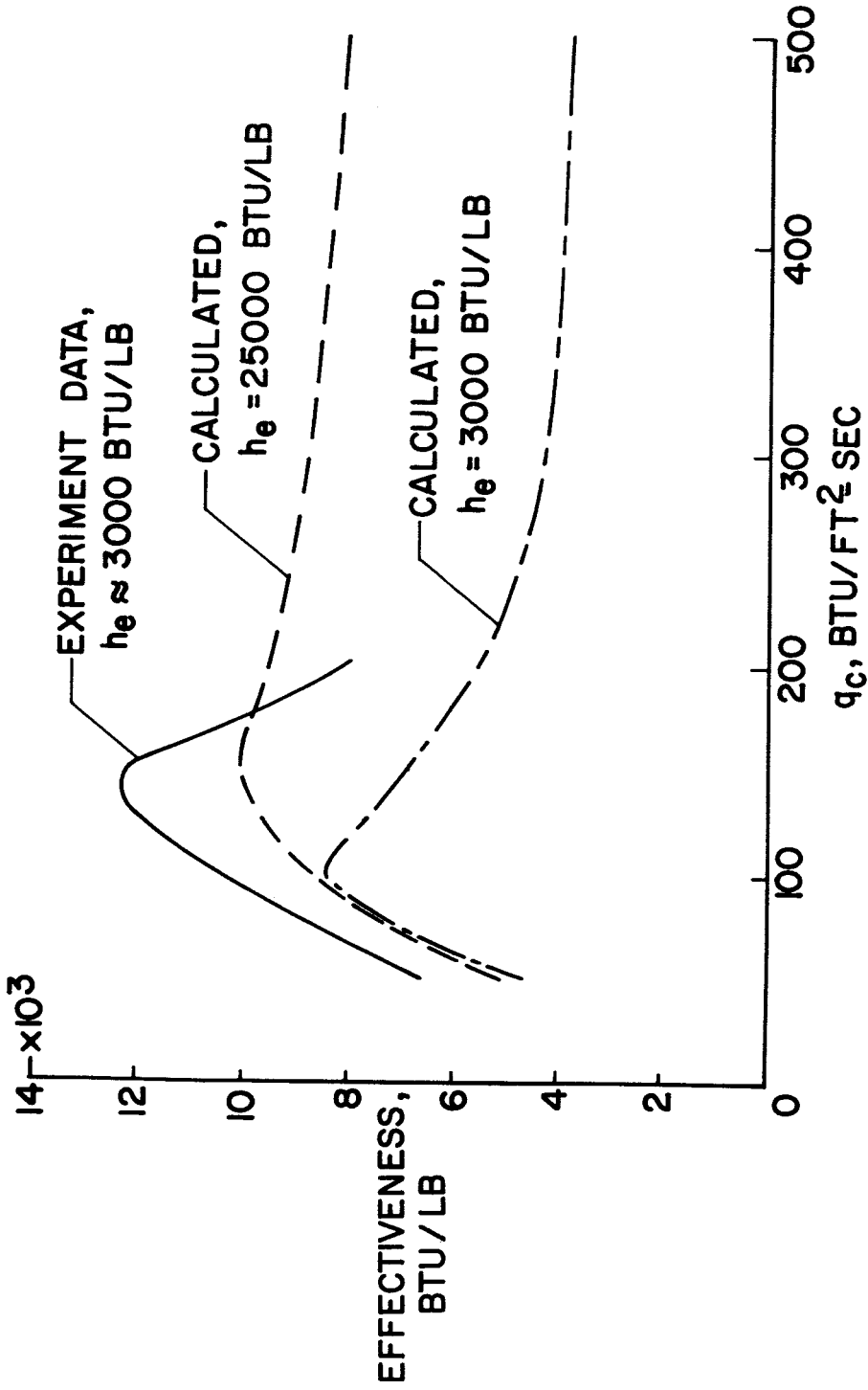


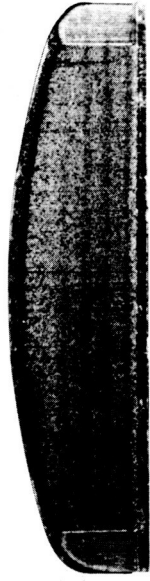
Figure 29.- The thermal effectiveness of a low-density silicone-resin ablator.



NASA

Figure 30.- The effect of heating rate on the performance of a silicone-resin ablator.

LOW DENSITY  
PHENOLIC-NYLON



LOW SHEAR,  
4 PSF

TEST TIME = 10 SEC



HIGH SHEAR,  
20 PSF

TEST TIME = 10 SEC

LOW DENSITY EPOXY RESIN  
GLASS REINFORCED



TEST TIME = 10 SEC



TEST TIME = 2.4 SEC

NASA

Figure 31.- An example of char removal by aerodynamic shear.

THERMAL INPUT:

$$\alpha q_R + q_{C, NET}$$

CHEMICAL INPUT:

$$\dot{m}(O_2)$$

MECHANICAL INPUT:

$$P_w \hat{n} + \tau_w \hat{\tau}$$

RELATIONS BETWEEN INPUTS:

$$\frac{q_{C, NET}}{h_e - h_w} \approx \frac{\dot{m}(O_2)}{C_e - C_w} \approx \frac{\tau_w}{u_e}$$

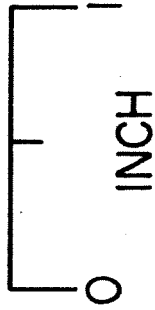
Figure 32.- The environmental inputs to an ablating surface.

	HIGH ENTHALPY	LOW ENTHALPY
CONDITIONS FOR SIMILARITY: ENTHALPY, BTU/LB HEATING RATE, BTU/FT <sup>2</sup> -SEC OXYGEN CONCENTRATION TEST DURATION, SEC	10,050 200 0.380 20.6	3600 150 0.116 27.4
TEST RESULTS: SURFACE RECESSON, IN. CHAR THICKNESS, IN. THICKNESS DEGRADED, IN.	0.03 0.08 0.11	0.03 0.09 0.12

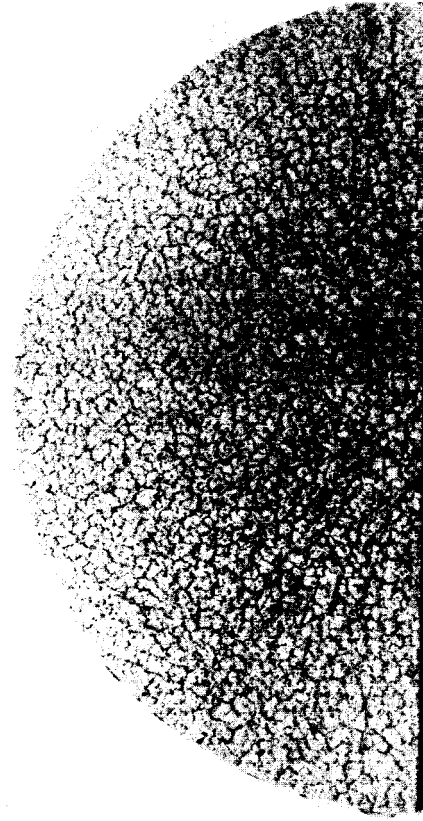
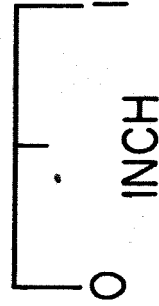
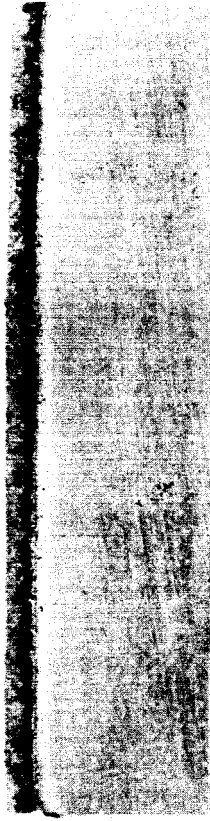
NASA

Figure 33.- The production of similar ablation test results in dissimilar test environments.

HIGH ENTHALPY TEST  
h = 10,050 BTU/LB

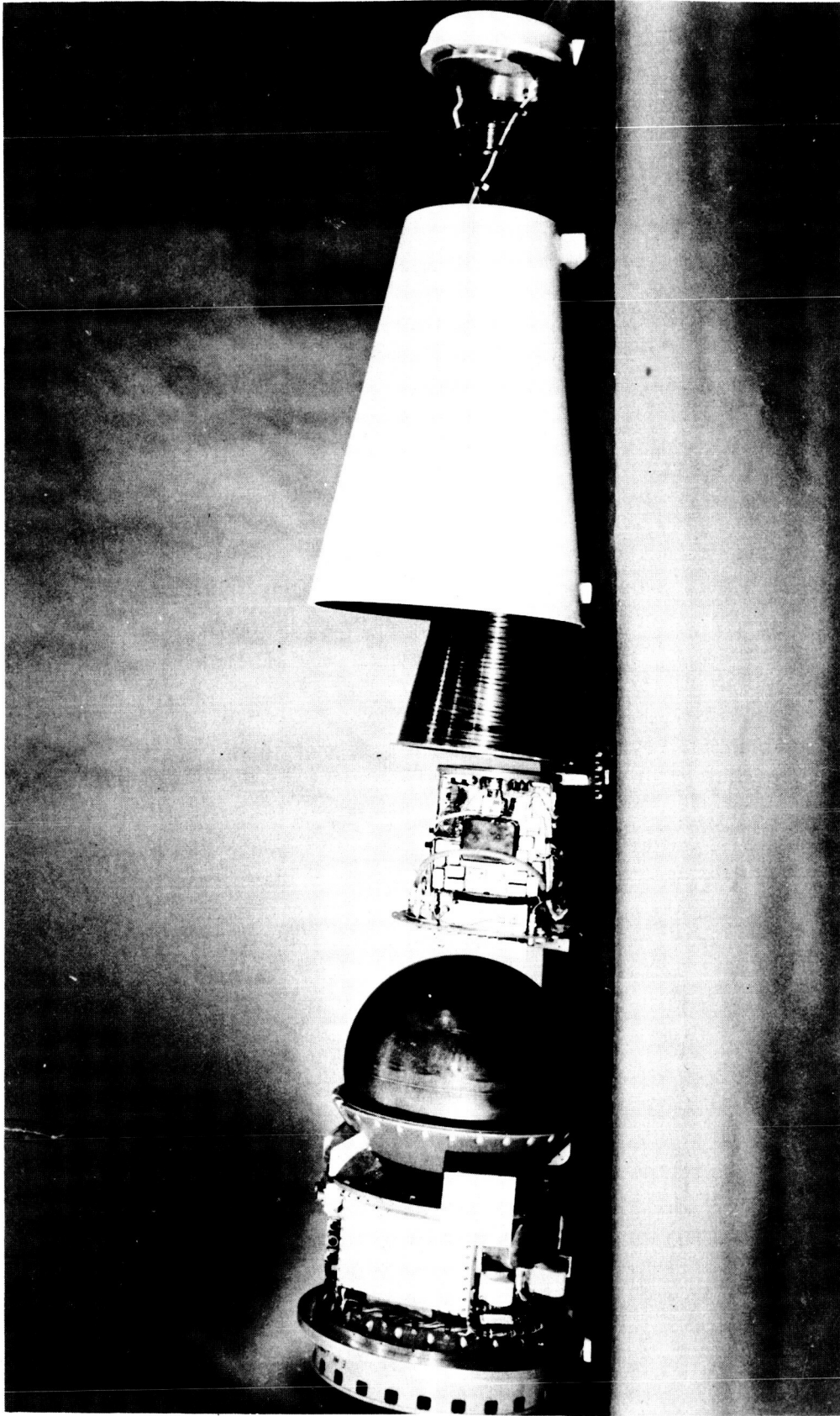


LOW ENTHALPY TEST  
h = 3,600 BTU/LB



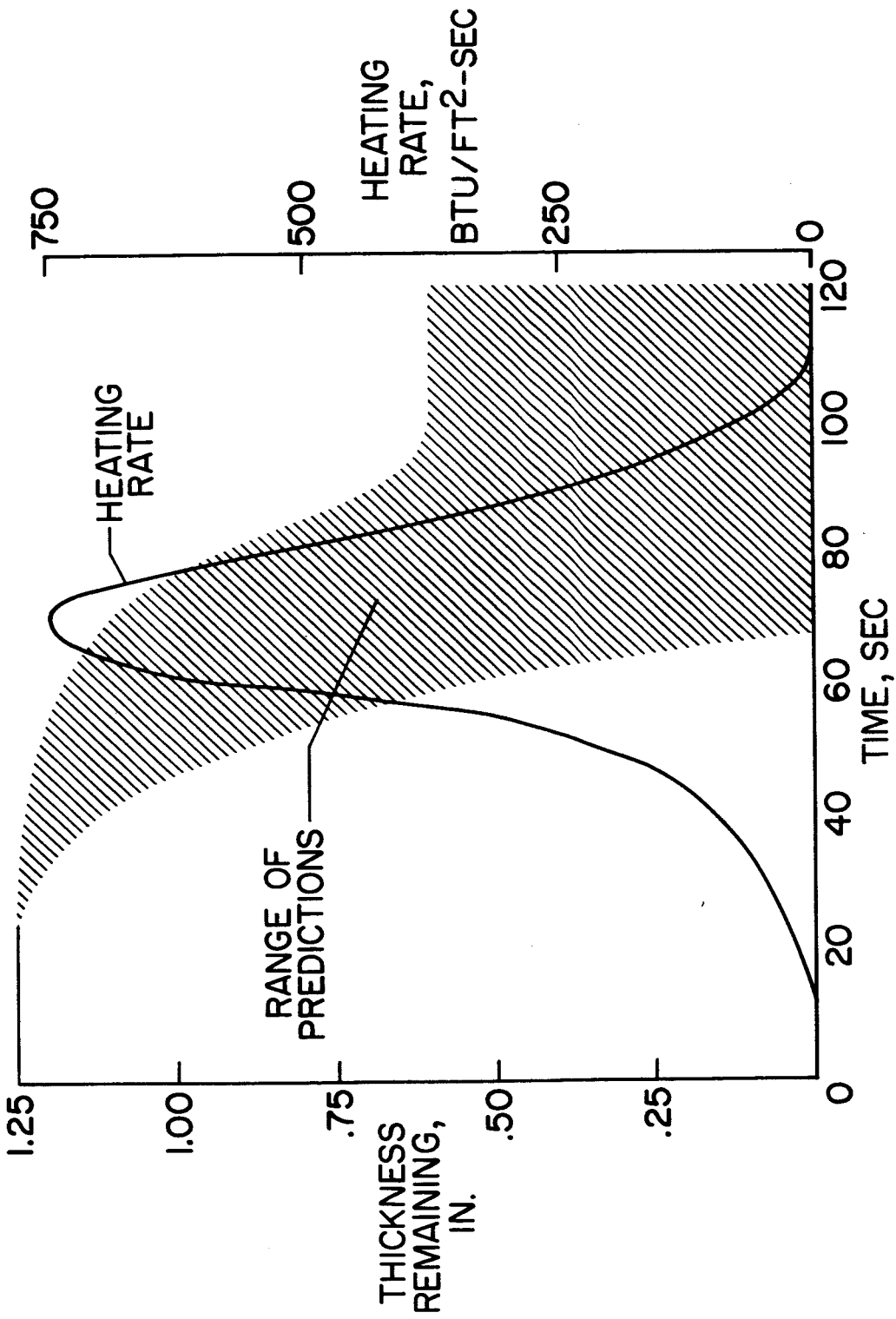
NASA

Figure 34.- Sectioned specimens showing similar results from dissimilar environments.



NASA

Figure 35.- Components of a Langley Research Center Scout Reentry Project payload.



NASA

Figure 36.- Empirical predictions of a heat-shield performance for a Scout Reentry Project payload.